I&EC research
Industrial & Engineering Chemistry Research

Article

Optimal Reactor Design via Flux Profile Analysis for an Integrated Hydroformylation Process

Nicolas M Kaiser, Michael Jokiel, Kevin McBride, Robert J. Flassig, and Kai Sundmacher

Ind. Eng. Chem. Res., **Just Accepted Manuscript** • DOI: 10.1021/acs.iecr.7b01939 • Publication Date (Web): 08 Sep 2017

ACS Publications

Industrial & Engineering Chemistry Research is published by the American Chemical Society. 1155 Sixteenth Street N.W., Washington, DC 20036

Optimal Reactor Design via Flux Profile Analysis for an Integrated Hydroformylation Process

Nicolas M. Kaiser[a], Michael Jokiel[b], Kevin McBride[b], Robert J. Flassig[b], Kai Sundmacher[a,b]

[a] Otto-von-Guericke-University Magdeburg, Department Process Systems Engineering, Universitätsplatz 2, D-39106 Magdeburg, Germany

[b] Max Planck Institute for Dynamics of Complex Technical Systems, Department Process Systems Engineering, Sandtorstr.1, D-39106 Magdeburg, Germany

Abstract

Different operational modes, various scales and complex phenomena make the design of a chemical process a challenging task. Besides conducting basic lab experiments and deriving fundamental kinetic and thermodynamic models, a crucial task within the entire process design is the synthesis of an optimal reactor-network constituting the core of a chemical process. However, instead of directly up-scaling the process to large devices, it is wise to investigate process characteristics on miniplant-scale.

For an existing miniplant for the hydroformylation of 1-dodecene using a rhodium catalyst and a thermomorphic solvent system for catalyst recovery, two optimized reactor designs are derived. Suitable reactor-networks were synthesized by applying the *Flux Profile Analysis* approach introduced in Kaiser et al. (2017). The combination of a first reactor with dynamic/distributed control options and a subsequent back-mixed CSTR arose to be the most promising configurations. The technical design under miniplant conditions were carried out for two possible realizations of this network, namely (i) a continuous flow reactor and (ii) a periodically operated semibatch reactor, both followed by the existing CSTR which was originally operated in the miniplant. An optimization of the two optimal reactor configurations within an overall process including a

liquid-liquid phase separation for catalyst recovery and a distillation column for separating the solvents and reactant evinced a selectivity w.r.t. the linear aldehyde around 94 % and a conversion around 98 %. This is a large improvement of the process performance of 24 % linear aldehyde selectivity and 40 % conversion when using the existing CSTR.

Keywords: Reactor-network synthesis, Reactor design, Optimization, Hydroformylation, Miniplant, Thermomorphic Solvent Systems

1. Introduction

Process systems development is a very challenging task owing to physico-chemical phenomena on different time and length scales. It is important to create an effective synergy of computational and experimental methods that incorporate all these scales. However, in practice these methods are often used apart from each other. To establish an interdisciplinary multi-scale process development, the Collaborative Research Centre TRR63 InPROMPT of the German Research Foundation was founded. In this transregional cooperation the design of an optimal reactor concept, the development of optimal separation techniques, and the assembly and experimental investigation in a miniplant-scale experimental setup is carried out for the hydroformylation of 1-dodecene in innovative solvent systems. A special feature within this project is the focus on miniplant-scale experiments which allow for consideration of recycle effects, effects by continuous operation and scale-up effects. In contrast to a pilot-scale, it is not a downsized copy of the later production plant, but a highly flexible, experimental setup including various possible scenarios of the future process[1].

The hydroformylation is a large-volume homogeneously catalyzed reaction which functionalizes olefins by insertion of hydrogen and carbon monoxide to form aldehydes, which are produced as a mixture of linear (n) and branched (iso) forms. The demand of linear aldehydes is much higher due to their higher biodegradability. The process is catalyzed by active transition metals in combination with ligands which provide a much higher stereo- and chemo-selectivity w.r.t. the desired linear aldehyde. The high activity and selectivity of rhodium-based catalysts enables the hydroformylation reaction to be conducted at more moderate operating conditions

than with other transition metals such as cobalt. However, rhodium and the associated ligands are very expensive and a very high catalyst recovery is indispensable for an economically profitable process. Several new solvent systems are under investigation in order to enable an efficient catalyst and ligand separation, e.g. thermomorphic solvent systems (TMS)[2], micellar solvent systems[3], gas-expanded liquids[4], and ionic liquids[5].

The presented process development is carried out for the hydroformylation of 1-dodecene in a thermomorphic solvent system of n-decane and n-,n-dimethylformamide[6]. Thermomorphic solvent systems consist of a polar and an apolar solvent. Under reaction conditions they build a homogeneous phase. For the separation after the reaction is complete, a phase split is induced by reducing the temperature. The polar solvent dissolves the catalyst and is recycled to the reactor inlet, whereby the apolar phase dissolves products and remaining reactants and is further separated downstream. Several studies on this process are published and provide a very good basis for a process design procedure. Kiedorf et al.[7] and Hentschel et al.[8] determined a reaction network and corresponding reaction rates for the aforementioned process catalyzed by a rhodium(acac)$(CO)_2$/Biphephos catalyst complex. Hentschel et al.[9] and McBride et al.[10] conducted overall process cost optimizations focusing on the design of an optimal reaction section and the design of the optimal separation configuration, respectively. Within the latter work a Kriging surrogate model for the liquid-liquid phase separation of the TMS system is developed as well, which is used in this work. The development of a miniplant process and its experimental investigation is done for a configuration of a single CSTR and a liquid-liquid phase separation with closed catalyst recycle in Dreimann et al.[11], and with a subsequent distillation column and additional recycle of byproducts and remaining reactants in Dreimann et al.[12].

The target of the present work is the design of an optimal reactor concept for the existing miniplant described in Dreimann et al.[12]. Therefore, all technical limitations and requirements of the miniplant are taken into account. The optimal reactor concept is synthesized using the *Flux Profile Analysis (FPA),* introduced in Kaiser et al.[13], which allows for synthesizing reactor-networks based on a dynamic optimization framework. This approach has its origin in the methodology of *Elementary Process Functions (EPF)* developed by Freund and Sundmacher[14]. Its key concept is the optimal control of mass and energy fluxes imposed on a Lagrangian element in its thermodynamic state space. The FPA uses this concept to identify characteristic control sections

based on optimal control fluxes along the reaction progress which can be translated on the one hand into back-mixed, back-mixing free and distributed controlled reactor types, and on the other hand be classified regarding their optimal heating/cooling policies. In addition benefits from recycling are revealed.

In Section 2 the FPA is carried out step by step for the synthesis of suitable reactor-network candidates for the aforementioned hydroformylation process. The resulting reactor-network candidates are compared and the most promising one is designed in detail using the miniplant conditions in Section 3. In Section 4 the resulting optimal reactor designs are embedded in a model of the miniplant including a Kriging surrogate model for the liquid-liquid phase separation and a short-cut model for the distillation column considering both catalyst recycle and byproduct recycle to be closed. Thereby, the performance of the optimal reactor designs can be compared to the performance of the existing setup with a single CSTR. Finally, the results are discussed and concluded in Sections 5 and 6, respectively.

2. Reactor Network Synthesis

2.1 Choice of Desired Process Indices

The derivation of an optimal reactor network for the aforementioned hydroformylation of 1-dodecene in a thermomorphic solvent system is done via the *Flux Profile Analysis*[13]. In general, a process unit can only be designed using given requirements and/or performance windows. Therefore, some reasonable assumptions for the desired reactor performance have to be made in advance. A closer look at previous work on this hydroformylation process shows that the maximization of the chemo-selectivity w.r.t. to the linear aldehyde tridecanal is a suitable objective function, since the process underlies a classical selectivity problem for the desired product[9]. Moreover, a stereo-selectivity problem arises due to the formation of linear and branched aldehyde tridecanal and 2-methyl-dodecanal, respectively. Hentschel et al.[9] came to the conclusion that a high ratio of linear to branched aldehydes ($n/iso\ ratio$) is important to reduce the separation effort and to avoid an additional distillation column for the separation of those isomers. From these insights it is concluded that the maximization of the selectivity towards tridecanal S_{nC13al} should be chosen as the objective function and to impose a constraint for the $n/iso\ ratio$ ratio ensuring it remains at least 95 %. In addition to the selectivity, the conversion is an important performance measure for the process. A high conversion has the advantage of smaller recycle streams of the remaining reactant to the reactor inlet. However, as Kaiser et al.[14] showed in their uncertainty quantification, the uncertainty of the predicted reactor performance increases drastically for conversions higher than 99 %. To ensure a good trade-off between high conversion and small loss in predictive power of the reactor design, the reactor network synthesis is carried out for conversions of 1-dodecene X_{nC12en} between 90 % and 99 %. Summarizing the aforementioned requirements, the optimization goal is given as:

$$\max S_{nC13al}$$

$$s.t.\ 90\% \leq X_{nC12en} \leq 99\%$$

$$n/iso\ ratio\ \geq 95\%.$$

2.2 Flux Profile Analysis for Reactor-Network Synthesis

For these desired performance indices the reactor-network synthesis is carried out. The *Flux Profile Analysis* approach follows a three-step procedure. The first step consists of solving a dynamic optimization problem to determine the optimal dosing and temperature control profiles. In the second step these profiles are subdivided in specific sections. Finally, the newly defined sections are associated to ideal reactor types in order to allow for the construction of candidate reactor networks.

2.2.1 Step 1: Dynamic Optimization

The dynamic optimization is based on the idea of a batch reactor combined with an ideal separator and storage tanks for all components α. From these storage tanks, specific components can be optimally dosed into the batch reactor along the reaction time. The mass balances of the batch reactor and the storage tanks are given in Eq. (A1) and Eq. (A2), respectively. The kinetics and thermodynamic relations for solubilities and densities are adopted from Hentschel et al.[8] and are also given in the Appendix (Eqs. (A3) – (A16)). As Kaiser et al.[13] stated, the *Flux Profile Analysis* requires additional constraints on reactant use and product dosing, see Eqs. (A17) – (A18).

The resulting dynamic optimization problem (DOP) reads:

$$\max_{j_\alpha(t),T(t),p_{CO}(t),p_{H_2}(t),t_f} \left\{S_{nC13al}(t_f)\right\} \qquad \text{(DOP)}$$

s.t. Component mass balances: Eq. (A1)

Storage mass balances: Eq. (A2)

Reaction kinetics: Eqs. (A3) – (A12)

Constitutive equations: Eqs. (A13) – (A14)

Gas solubilities: Eqs. (A15) – (A16)

Dosing constraints: Eqs. (A17) – (A18)

Inequality path constraints: $j_\alpha(t) \geq 0, n_\alpha(t) \geq 0, n_{\alpha,st}(t) \geq 0,$

$$10\ \text{bar} \leq p_{total} = p_{CO} + p_{H_2} \leq 20\ \text{bar},$$

$$363.15\ \text{K} \leq T \leq 388.15\ \text{K},$$

Terminal constraints: $n_{\alpha,st}(t_f) \leq n_{\alpha,st}^{max} = 0, \qquad n_{\alpha}(0) = 0, \quad \forall \alpha \in CH,$

$$n_{\alpha,st}(0) = 1, \forall \alpha \in CH\ ,$$

$$t_f \leq 300\ \text{min},$$

$$90\ \% \leq X_{nC12en} = \frac{n_{nC12en}(t=0) - n_{nC12en}(t_f)}{n_{nC12en}(t=0)} \leq 99\ \%,$$

$$n/iso\ ratio = \frac{n_{nC13al}(t_f)}{n_{nC13al}(t_f) + n_{iC13al}(t_f)} \geq 95\%.$$

The final reaction time is restricted to a maximum value of $t_f^{max} = 300\ \text{min}$ to avoid oversized reactor concepts and to stay within the miniplant-scale. The temperature T and the total pressure p_{total} have lower and upper bounds due to the valid ranges in which the kinetics have been determined.

The *Flux Profile Analysis* can be performed considering the dosing of reactants and products independently of each other or simultaneously. In the first case only the effect of reactant concentration is investigated ignoring the impact of recycle. If the product dosing is included, the benefit of recycles and/or back-mixing is also considered. Since the target of the present reactor design study is to find an optimal reactor concept which leads to high performance with and without closed product recycle, both cases are investigated. The DOP is carried out for the minimum and maximum of the desired conversion range of 1-dodecene to check the influence of conversion on the optimal reactor concept. The four resulting cases are:

- Case 2.1: Only reactant dosing, $X = 90\ \%$
- Case 2.2: Only reactant dosing, $X = 99\ \%$
- Case 2.3: Reactant and product dosing, $X = 90\ \%$
- Case 2.4: Reactant and product dosing, $X = 99\ \%$.

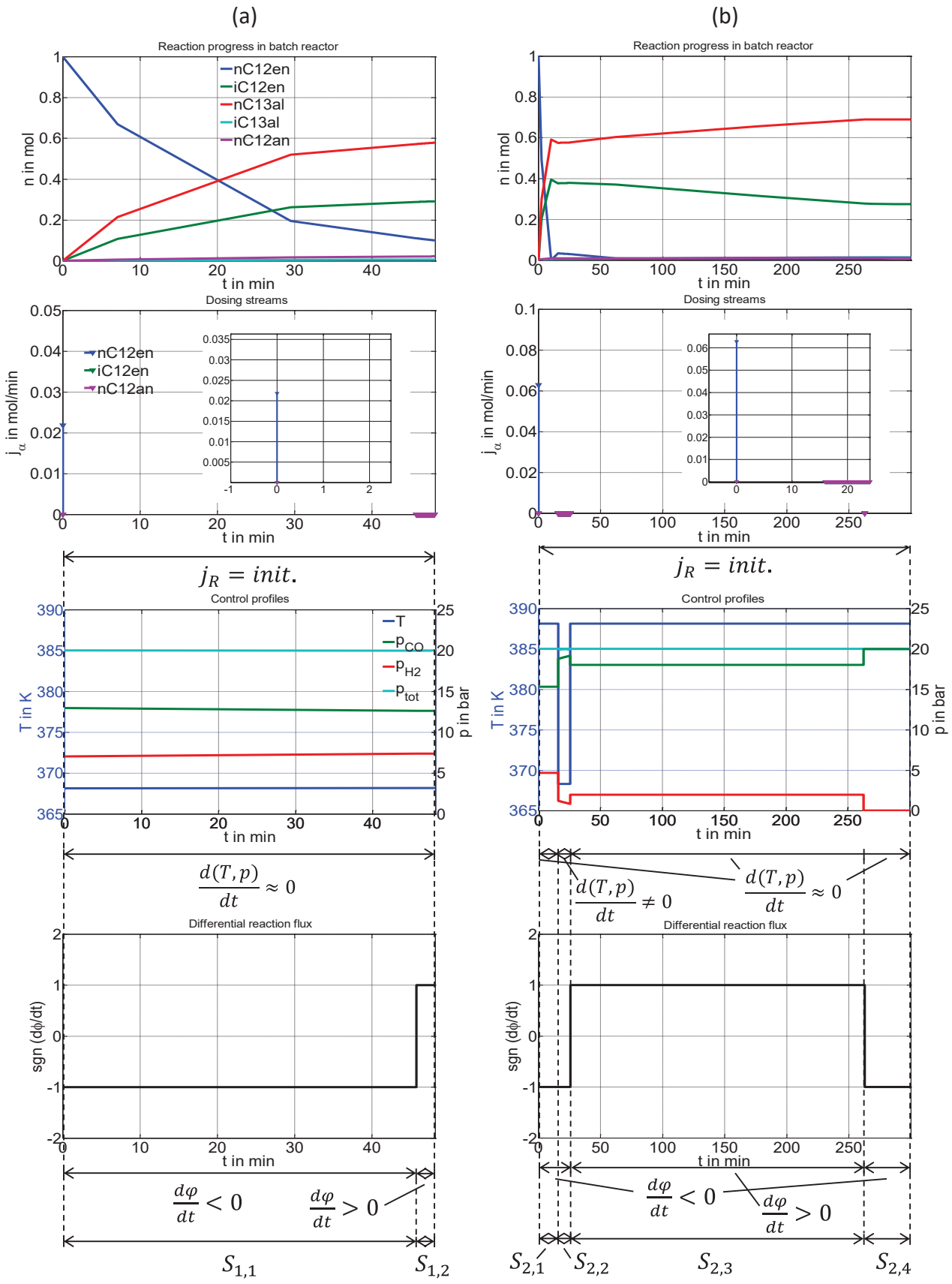

Figure 1: *Flux Profile Analysis* for case 2.1 (a) and case 2.2 (b): Molar-holdups $\boldsymbol{n_\alpha}$, dosing streams $\boldsymbol{j_\alpha}$, control profiles $\boldsymbol{T}$ and $\boldsymbol{p}$, differential reaction flux $\boldsymbol{d\varphi/dt}$.

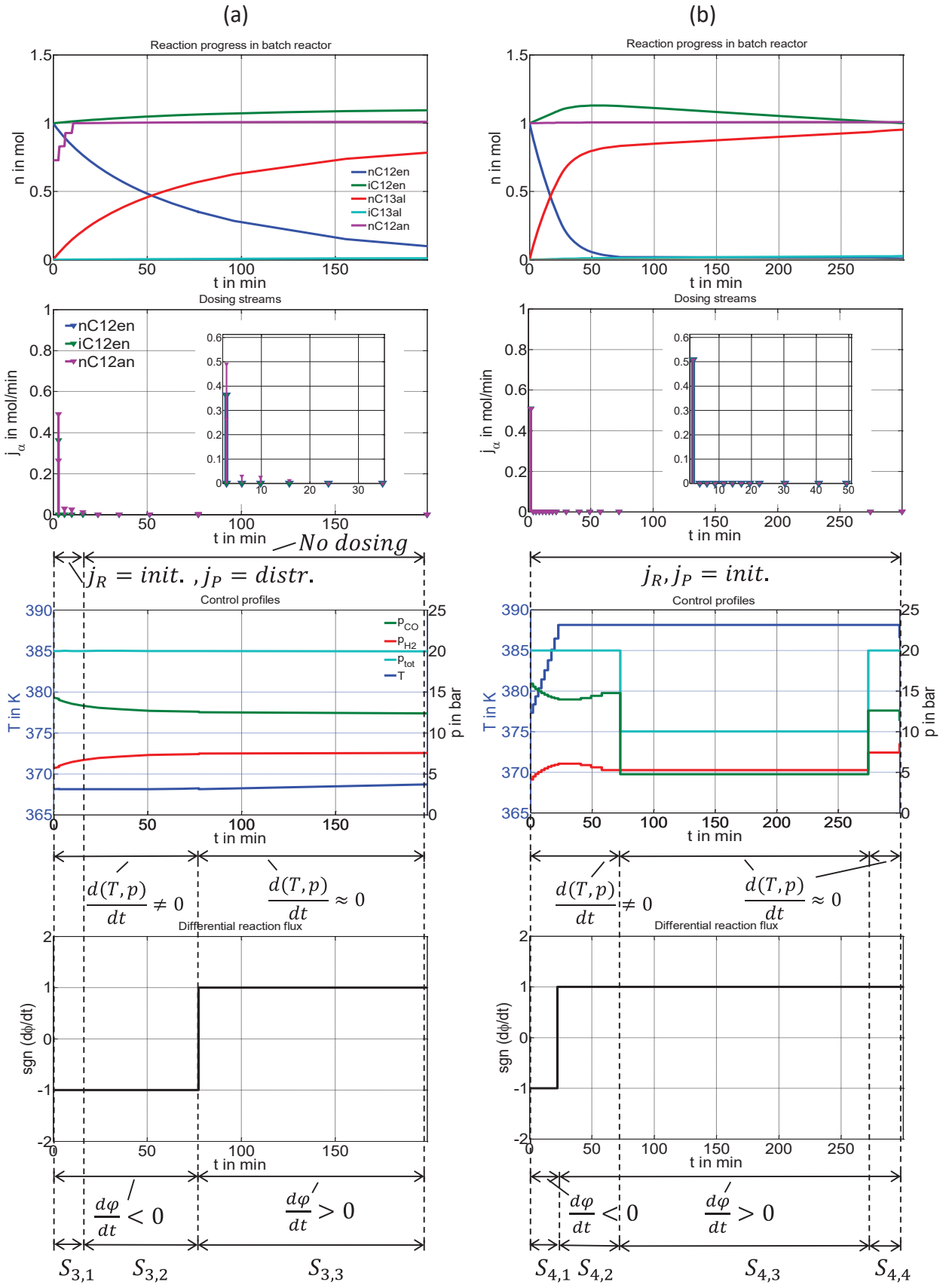

Figure 2: *Flux Profile Analysis* for case 2.3 (a) and case 2.4 (b): Molar-holdups $\boldsymbol{n_\alpha}$, dosing streams $\boldsymbol{j_\alpha}$, control profiles $\boldsymbol{T}$ and $\boldsymbol{p}$, differential reaction flux $\boldsymbol{d\varphi/dt}$.

2.2.2 Step 2: Subdivision in Specific Sections

The results of the four dynamic optimization cases are shown in Fig. 1 and Fig. 2. For each case the reaction progress in the batch reactor, the dosing streams, the control profiles of temperature and partial pressures, and the differential reaction flux along the reaction time is illustrated. Although CO and H_2 are also reactants and their partial pressures are affected by dosing, they are treated as control variables and not as dosing of reactants. This is because their dosing does not provide information for the analysis of the mixing and back-mixing characteristics of the process.

2.2.3 Step 3: Association to Ideal Reactor Types

For each of the optimization cases the identified subsections are analyzed individually and mapped to reactor types which are able to realize the characteristics of the corresponding section.

- Case 2.1: Only reactant dosing, $X = 90\ \%$

As one can see in Fig. 1 (a) the dosing of reactant occurs only in the beginning of the reaction and the temperature and partial pressures remains almost constant. The differential reaction flux shows two sections: the first is of negative order and the second of positive order. The latter identifies a benefit of back-mixing for this section of the reaction. Suitable reactor units for the two identified sections are derived from the FPA look-up table of Kaiser et al.[13]. The reactant dosing in $S_{1,1}$ can be easily realized by a plug flow reactor (PFR). However, to maintain the constant partial pressures a side dosing of gas is necessary and, thus, a distributed sidestream reactor (DSR) is indispensable. $S_{1,2}$ is due to its back-mixing benefit best realized by a continuous stirred tank reactor (CSTR). The resulting reactor-network candidate is illustrated in Fig. 3 (a).

- Case 2.2: Only reactant dosing, $X = 99\ \%$

The optimization results in Fig. 1 (b) indicate again only an initial reactant dosing and, due to the assumption of this case, no product dosing. The control profiles of temperature and partial pressures

are constant at the beginning ($S_{2,1}$) followed by a section of dynamic adaptation of partial pressures ($S_{2,2}$). After that, two sections of constant control profile occur ($S_{2,3}$, $S_{2,4}$). The differential reaction flux is of negative order in the first two control sections, of positive order in the third section, and again negative in the final, fourth control section. The complete initial dosing of reactant and the negative gradient of the differential reaction flux indicates a PFR behavior. Again, the dosing of gas is necessary and hence a DSR is chosen. The first and second control sections ($S_{2,1}$, $S_{2,2}$) are rather small in comparison to sections three and four. Thus, they are merged into one section with dynamic control of temperature and partial pressure. Section $S_{2,3}$ has no reactant dosing, constant control profiles and a differential reaction flux of positive order pointing towards a CSTR configuration. Following the same reasoning behind reaction section 1, the last section S_4 is also realized in a DSR. The resulting reactor-network candidate is depicted in Fig. 3 (b).

- Case 2.3: Reactant and product dosing, $X = 90\ \%$

As Fig. 2 (a) shows, the reactant is dosed initially and the product is dosed intermittently within the first section. In the second section no dosing occurs. The temperature control remains almost constant along the entire reaction time which is in contrast to the partial pressures which change in the first reaction section and then remain almost constant in the second reaction section. The gradient of differential reaction flux is negative in the beginning and positive at the end of the reaction time. The first reaction section, $S_{3,1}$, with its distributed dosing, dynamic control of partial pressures, and negative gradient of the differential reaction flux, can be merged with the second section $S_{3,2}$ which shows the same characteristics except of there is dosing of the reactant. This newly merged reaction section is realized in a DSR. The remaining third reaction section, $S_{3,3}$, is again best suited as a CSTR due to its constant control and positive order of differential reaction flux. This results in the same reactor-network candidate determined for case 2.1 which was illustrated in Fig. 3 (a).

- Case 2.4: Reactant and product dosing, $X = 99\ \%$

Again, the reactant and product are dosed initially, see Fig. 2 (b). The temperature and partial pressure profiles show that dynamic control is required in the first section followed by two sections requiring constant control. The change of differential reaction flux is negative in the relatively small first section and positive in the second, longer section. This suggests that there are overall four different reaction sections. The first of these, $S_{4,1}$, has the initial dosing of the reactant and products, a dynamic change in temperature and partial pressures, and a negative order of the differential reaction flux. This is then best realized in a DSR. The second section, $S_{4,2}$, has a positive gradient of the differential reaction flux, indicating that back-mixing would be beneficial, but requires a slightly dynamic control of the partial pressures. The latter is approximated as being constant so that this section can be realized in a CSTR. Sections $S_{4,3}$ and $S_{4,4}$ are also realized in CSTRs with different pressure levels. Hence, the four sections are associated with a DSR and 3 CSTRs leading to the reactor-network candidate illustrated in Fig. 3 (c).

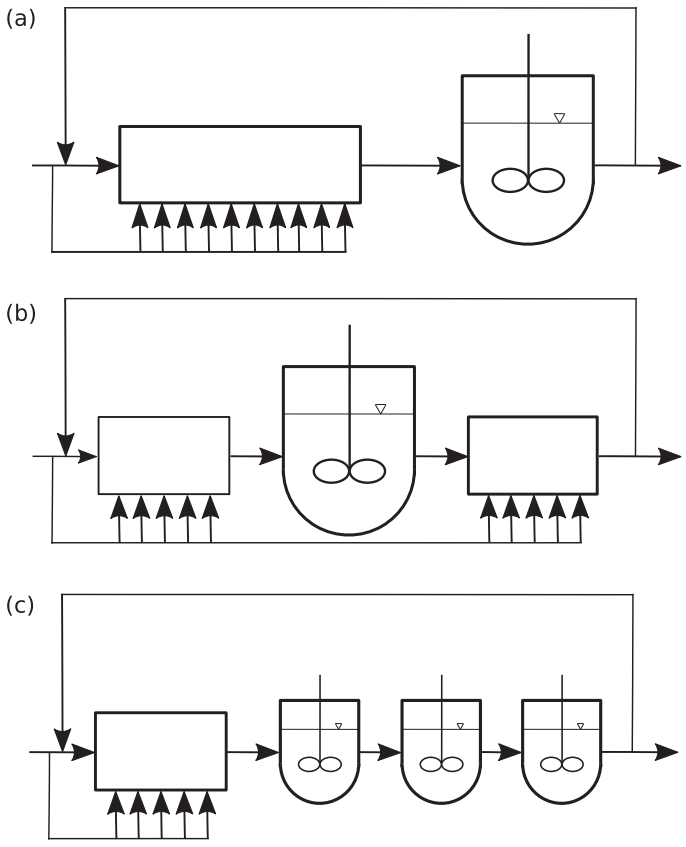

Figure 3: (a) DSR+CSTR reactor-network resulting from case 2.1; (b) DSR+CSTR+DSR reactor-network resulting from case 2.2; (c) DSR+CSTR+CSTR+CSTR reactor-network resulting from case 2.4.

The *Flux Profile Analysis* leads to three reactor-network candidates depicted in Fig. 3. Furthermore, it is possible to realize the process with only one DSR corresponding to the optimized batch reactor with intermediate dosing. This is analogous to the application of the EPF method in e.g. Hentschel et al.[9]. In the next step, these four options have to be analyzed to identify the most promising network and the expected trade-off between performance and network size.

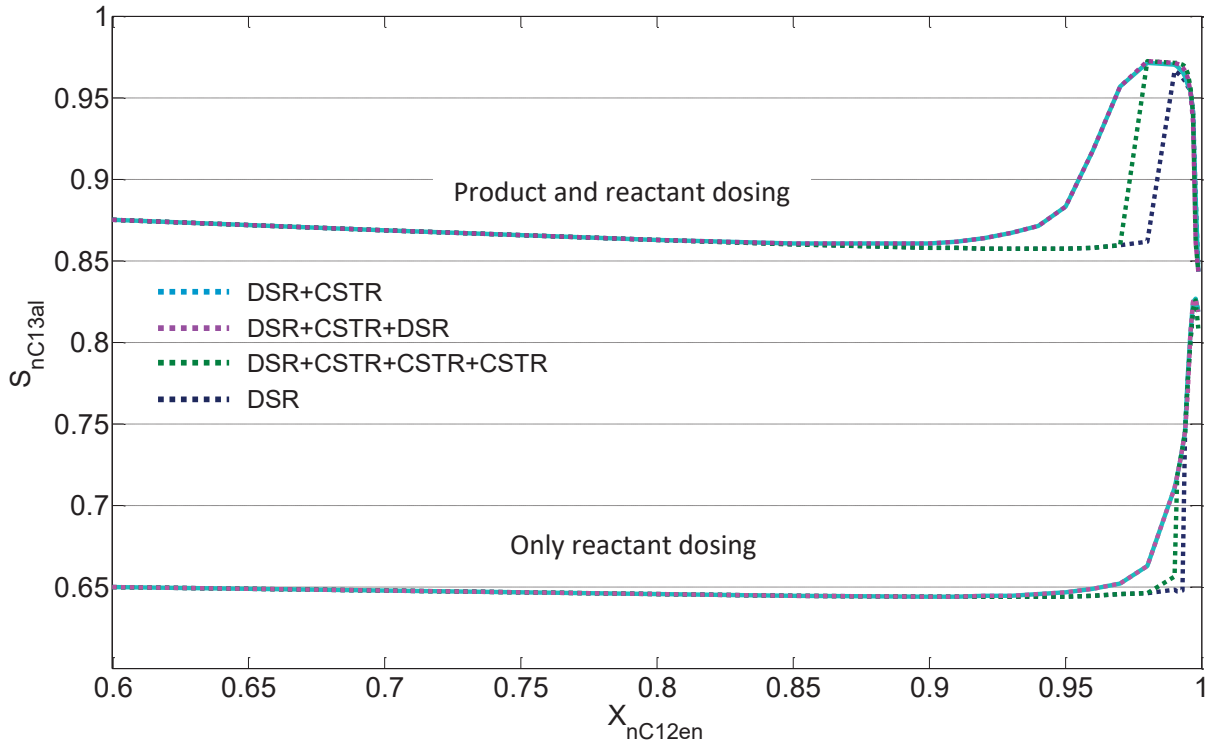

Figure 4: Selectivity w.r.t. tridecanal (nC13al) over conversion of 1-dodecene (nC12en) for the case of only reactant dosing (bottom) and with product and reactant dosing (top).

2.2.4 Comparison of Reactor-Network Candidates

To compare the four reactor-network candidates defined in the previous section, a typical illustration in reactor engineering is chosen: the selectivity w.r.t. to the desired product is plotted against the conversion of

the main reactant. This S/X diagram allows one to identify the candidate which has the highest product yield for the entire range of conversion or at least a reasonable subsection thereof (see Fig. 4).

The dotted lines at the bottom of Fig. 4 correspond to cases 2.1 and 2.2 where only reactant dosing occurs, whereas the dotted lines at the top of the figure correspond to cases 2.3 and 2.4 with both reactant and product dosing. The network candidate with only one DSR (blue) has the worst potential for both assumptions. In the conversion range between $90\ \% \leq X_{nC12en} \leq 99\ \%$ all other candidates show higher selectivities w.r.t. the linear aldehyde S_{nC13al}. The realization with a DSR and a subsequent CSTR (cyan) shows much higher selectivities in the aforementioned conversion range due to the back-mixing in the second reactor. The same is valid for the DSR+CSTR+DSR network (pink), whereby the gain in selectivity in comparison to the candidate with one CSTR at the end is very small. The green line illustrates the result for the case of a DSR and 3 CSTRs. Here, some suboptimal solutions are found, since this network has the same potential as the DSR+CSTR network, but does not perform as well at all conversions. Moreover, it has a slightly higher potential for high conversions of 1-dodecene $X_{nC12en} \geq 99\ \%$. The results indicate that the two larger candidates, namely the DSR+CSTR+DSR and the DSR+CSTR+CSTR+CSTR networks, have only a very small benefit when compared to the shorter DSR+CSTR network. Therefore both candidates are not suitable choices. The reason might be, on the one hand, that the higher back-mixing effect with only one CSTR is much more beneficial than the different partial pressure levels in three different CSTRs and, on the other hand, that the DSR at the end of the process only covers a very small part of the entire conversion and thus has almost no effect. In contrast to these, the DSR+CSTR network has an unambiguous benefit in comparison to using a single DSR or, in discontinuous terms, a single semibatch reactor. Due to these results the DSR+CSTR network illustrated in Fig. 3 (a) is designed in more detail in the following section.

3. Reactor Design

After determining the most suitable reactor-network the next step is its technical realization for the operating conditions of the miniplant where the reactor concept is to be embedded.

3.1 Miniplant Conditions

The miniplant running the hydroformylation of 1-dodecene in a thermomorphic solvent system consisting of DMF and n-decane is described in detail in Zagajewski et al.[16] and Dreimann et al.[11,12]. The operating conditions such as feed stream composition, amount of catalyst, solvent composition, reactor volume etc. are adopted from Dreimann et al.[12] and summarized in Tab. 1.

Table 1: Operational conditions of hydroformylation miniplant

T_R	**90°C**
$w_{1-dodecene}$	0.16
$w_{n-decane}$	0.42
w_{DMF}	0.42
p_{total}	21 bar
CO/H_2	1:1
$n_{dodecene}/n_{Rh}$	4000/1
$n_{biphephos}/n_{Rh}$	5/1
T_S	5°C
$\dot{V}_{1-dodecene}$	32 ml/h
$\dot{V}_{n-decane}$	88 ml/h
$\dot{V}_{make-up}$	2.5 ml/h
$w_{DMF}^{make-up}$	0.9893
$w_{Rh(acac)(CO)_2}^{make-up}$	0.0001
$w_{Biphephos}^{make-up}$	0.0107
$\dot{V}_{feed}^{column}$	120 ml/h

The CSTR operated in the miniplant has a volume of $V_R = 1\,\mathrm{l}$ with a liquid hold-up of $\varepsilon_{liq} = 0.3$. The corresponding residence time for the given volume and volumetric inlet streams is approximately a third of the maximum reaction time ($\tau \approx 100$ min). This is also the value set for the dynamic optimization in Section 2. Thus, it is recommendable to use the embedded CSTR already in use in the miniplant as the second reactor in the optimal reactor-network. The volume and liquid hold-up of this CSTR are given as constraint for the following reactor design study.

3.2 Model Basis for Reactor Design Study

For the dynamic optimizations discussed in Section 2, the concept of a semibatch reactor with ideal separation and storage tanks was considered corresponding to the Lagrangian view of the EPF[15]. The following reactor design study considers a different and extended model in which the gas phase is balanced and the mass transfer between the gas phase and liquid phase is taken into account. Thus, gas dosing fluxes for H_2 and CO are added as control variables. For the cases with optimal initial product dosing, what corresponds to an ideal recycle of products and byproducts, an additional constraint is included (Eq. 1) ensuring that the initial product dosing does not exceed the corresponding product amount in the reactor outlet:

$$j_\alpha(z=0) \leq \dot{n}_\alpha^f, \quad \alpha \in \{CH\backslash nC12en\} \tag{1}$$

The balance equations for the different reactor types PFR, DSR, SBR, and CSTR are given in Eqs. (A19) – (A24), Eqs. (A19) – (A25), Eqs. (A26) – (A31), and Eqs. (A32) – (A34), respectively.

3.3 Possible Technical Approximations

The technical realization of the reactor-network proposed in Fig. 3 (a) is non-trivial. In the case where a completely continuously operated process is to be realized, the optimal control profiles for the DSR cannot be perfectly realized. This is because the optimally calculated control profiles are continuous but their realizations in a real reactor have to be discretely approximated. Therefore the following approximations are investigated:

- Case 3.1: PFR+CSTR with gas dosing only at the inlet of the PFR;
- Case 3.2: PFR+CSTR with gas dosing at the inlet of both reactors;
- Case 3.3: PFR+CSTR with one additional gas dosing along the PFR leading to a PFR+PFR+CSTR network.

A DSR section within a reactor-network can also be realized in a semibatch reactor (SBR) allowing for a continuous realization of the control profiles in time[13]. Thus, a forth, mixed batch-conti(nuous) realization is investigated:

- Case 3.4: SBR+CSTR corresponding to the optimal DSR+CSTR concept in a batch-conti process.

The results are illustrated in Fig. 5, again comparing the S/X behavior of the different cases for both instances (a) without product dosing and (b) with product dosing. The cyan lines correspond to case 3.1 and are obviously suffering from the missing gas control of the CSTR in the reactor-network. All other cases show increased selectivity over conversion for increased number of gas dosing points. Although cases 3.3 (pink) and 3.4 (blue) provide slightly better performances than case 3.2 (green), their realizations in a continuous operation would require substantially more effort. Thus, in case of a continuous operation case 3.2 (green) is sufficient enough to improve the process, especially for large conversions when compared to the use of a single CSTR. This is valid in the case of only reactant dosing and when byproduct is recycled.

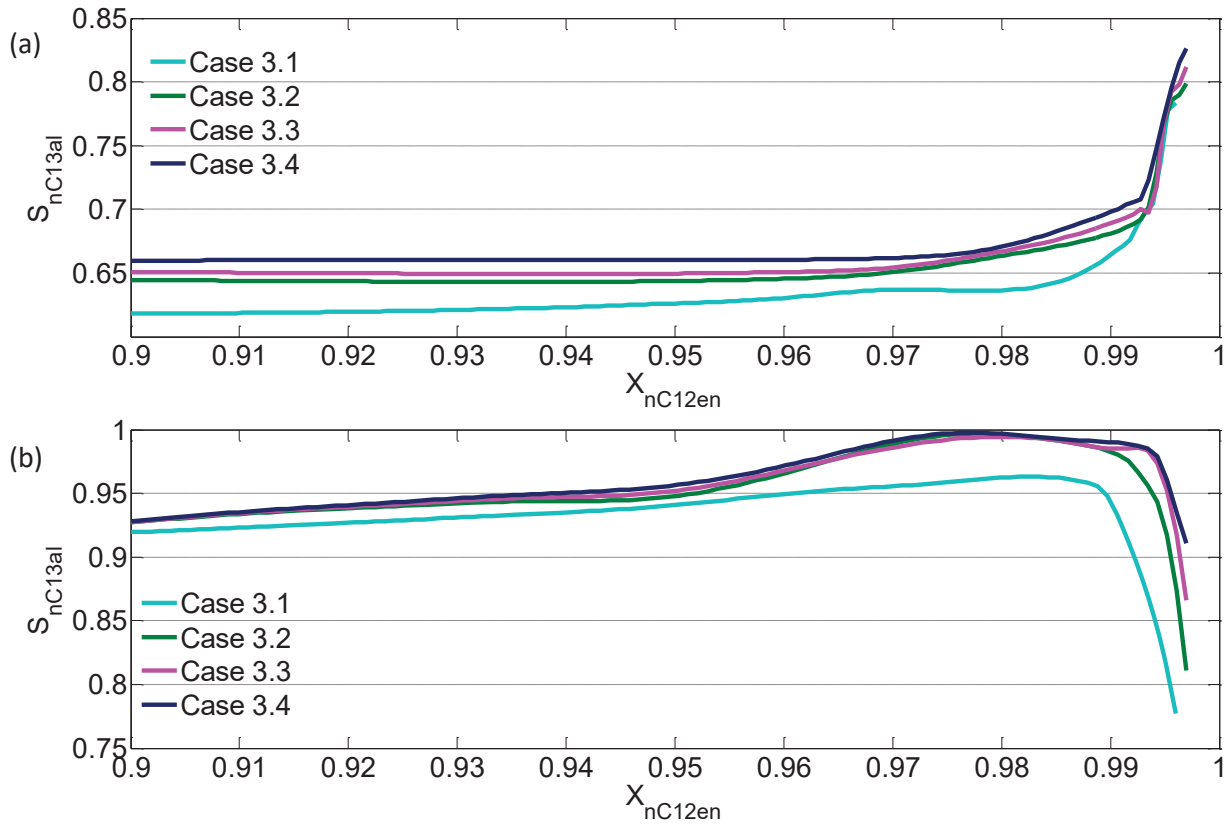

Figure 5: Selectivity w.r.t. tridecanal (nC13al) over conversion of 1-dodecene (nC12en) for the four realization cases (case 3.1 – cyan, case 3.2 – green, case 3.3 – pink, case 3.4 – blue) without product recycling (a), and with product recycling (b).

However, considering the batch-conti realization of the reactor, case 3.4 seems to be realizable with acceptable effort as well. To further investigate the differences of these two technical realizations, both are designed in more detail and optimized later within the complete miniplant operation discussed in Section 4.

As one can see in Fig. 5 the best conversion for reactor operation is at a conversion around $X_{nC12en} \approx 99\ \%$. At this point, the recycled system is at its maximum and the non-recycled is very close. Hence, the detailed reactor design is carried out for this conversion.

3.4 Detailed Design of Derived Technical Realizations

The design of case 3.2 and case 3.4 of the previous study face very different challenges. Case 3.2 consists of a plug flow reactor and a CSTR while case 3.4 consists of a semibatch reactor and a CSTR, whereby the CSTR in both cases has a predetermined size. In case 3.2 the focus is then to design a continuous flow reactor that approaches plug flow behavior. In contrast, case 3.4 has the challenge to combine the discontinuous first reactor with the continuously operated second reactor. As the temperature changes are rather moderate in a small range of $363.15\ \mathrm{K} \leq T \leq 388.15\ \mathrm{K}$ with the process being only slightly endothermic for both realizations, the heat transfer is not challenging. Since the hydroformylation is a gas-liquid multiphase process, it is important for both cases to investigate the mass transfer requirements in order to ensure that sufficient gas reactant is supplied as the reaction progresses. However, in case 3.4 this can be easily adjusted or controlled by the nature of the gas dispersion in the tank reactor. In case 3.2 this is more difficult, since it depends mainly on the flow regime and the characteristics of the resulting mixing.

3.4.1 Continuous Realization

The determination of a suitable flow regime is carried out based on predetermined minimum mixing conditions, i.e. a minimum volumetric mass transfer coefficient $k_L a$ and a minimum Péclet number ($Pé$) characterizing the axial dispersion. Aiming at identifying these measures, simulations of the reaction in a (equally sized) CSTR cascade model are carried out. This model allows for scanning the impact of different $Pé$ numbers on the reactor performance using the relations

$$\frac{Pé}{2} = N, \tag{2}$$

$$Pé = \frac{l*v}{D_{ax}}, \tag{3}$$

whereby N is the number of CSTRs in the cascade, l is the reactor length, v is the fluid velocity and D_{ax} is the axial dispersion coefficient. The simulations are carried out for both the case of product recycling and the case of no product recycling.

To identify the impact of the mass transfer rates on the performance of the PFR+CSTR network, the $k_L a$ value is set to different values between $0.3 \ldots 30\ \mathrm{min}^{-1}$holding the $Pé$ number constant at 100. Based on the results given in Fig. A1 (a), the minimum $k_L a$ value is set to $(k_L a)_{min} = 6\ \mathrm{min}^{-1}$, since for lower values the loss of selectivity w.r.t. tridecanal is higher than $\Delta S = 1\ \%$.

For the identification of the minimum $Pé$ number the $k_L a$ value is set to $100\ \mathrm{min}^{-1}$ and the $Pé$ number is varied between $4 \ldots 40$. The result shown in Fig. A1 (b) indicates a selectivity loss higher than $\Delta S = 1\ \%$ for $Pé$ numbers smaller than 10. Thus, the minimum value is set to $Pé_{min} = 10$.

The search for a suitable flow regime in the continuous flow reactor that satisfies the above requirements is strongly dependent on the range of dimensions, in particular the tube diameter. The previous optimization of the different technical realizations resulted in a residence time of $\tau_R = 300\ \mathrm{min}$ for the chosen cases 3.2 and 3.4 at $X_{nC12en} = 99\ \%$. Due to the given flow rate conditions (see Tab. 1) the residence time in the final CSTR is $\tau_R^{CSTR} \approx 90\ \mathrm{min}$. This corresponds to a residence time in the PFR of $\tau_R^{PFR} \approx 210\ \mathrm{min}$. Taking this residence time and the miniplant data in Tab. 1 into account and assuming a liquid hold-up of $\varepsilon_{liq}^{PFR} = 0.33$, the reactor volume of the PFR has to be $V_R^{PFR} \approx 2200\ \mathrm{ml}$.

Based on the miniplant conditions shown in Tab. 1 the overall volumetric flow rate of the liquid phase is $\dot{V}_{liq}^{in} \approx 200\ \mathrm{ml/h}$. With the given liquid hold-up the gas volumetric flow rate is $\dot{V}_{gas}^{in} \approx 400\ \mathrm{ml/h}$. To achieve the required $k_L a$ value and ensure small axial dispersion, an intermittent flow regime is used. It has the advantageous properties that (i) the axial dispersion within the phases is reduced significantly by the separation of the liquid bulks[18] and (ii) an internal recirculation within the liquid bulks is induced by the friction forces at the wall which strongly enhances the mass transfer[19]. The realization of this flow regime needs a small tube diameter guaranteeing a high ratio of surface tension forces to gravitational forces. Preliminary experimental investigations (see Appendix for detailed information) indicate that a tube with a diameter $d_{tube} = 3\ \mathrm{mm}$ provides a stable intermittent flow regime with a pressure drop of $\Delta p = 0.0017\ \mathrm{bar\ m^{-1}}$. This leads to a final reactor length of $l_{PFR} \approx 311\ \mathrm{m}$ and a pressure drop of $\Delta p = 0.5287\ \mathrm{bar}$ for the PFR. To allow for a manageable construction of the long tube reactor and its replacement within the miniplant setup, a bending of the tube to helices is favored. In addition to its compact construction, such a reactor configuration has the additional advantage of a uniform pressure loss due to the regular bending. The resulting setup is illustrated in Fig. 6 (b). The continuous reactor-network of the helically coiled tube reactor and the CSTR has no special operational conditions. The continuous flow reactor is heated by heating tapes and is well isolated. This allows for realizing various temperature zones.

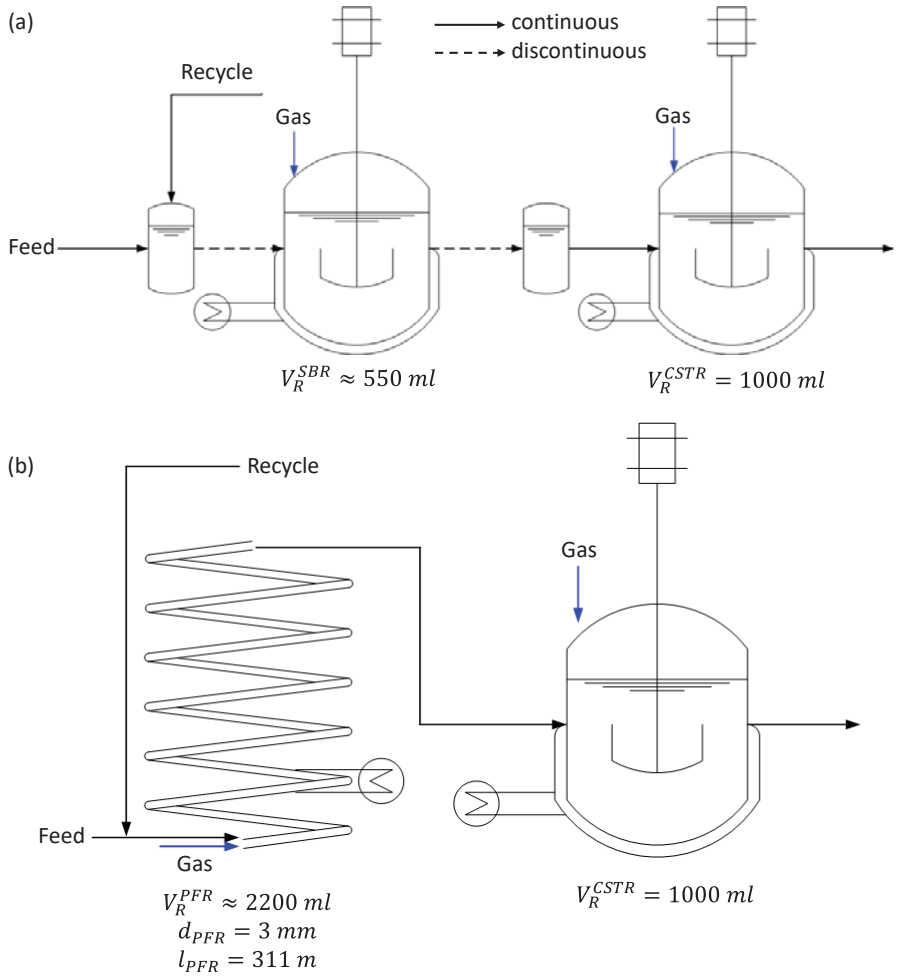

Figure 6: (a) SBR+CSTR network for batch-conti realization with two buffer tanks for maintaining a continuous operation; (b) Helically coiled tube reactor + CSTR network for pure continuous operation.

3.4.2 Batch-Continuous Realization

The realization of the hydroformylation process with the reactor-network given in case 2.4 of Section 2, namely the SBR+CSTR network, is of a different nature. The connection of a discontinuous and continuous reactor requires a buffer tank between the reactors, and in case of recycle also in front of the SBR. The SBR itself is already free of axial dispersion and its mass transfer can be adjusted by the stirrer type and speed. For the present realization, a gassing stirrer is used. In the existing CSTR of the miniplant a blade stirrer is installed which allows only smaller liquid hold-ups. Due to the use of a gassing stirrer the liquid hold-up can be increased to $\varepsilon_{liq}^{SBR} = 0.66$ [20].

The recycle streams are collected continuously in the heated upstream buffer tank and mixed with a continuous make-up stream of solvents and catalyst. This vessel has to be pressurized with synthesis gas to prevent catalyst deactivation. The reactant is fed into the SBR from an additional vessel, to prevent reaction taking place in the upstream buffer tank. The SBR is then fed batch-wise. After the final batch time has been reached, the reaction mixture is led into the second buffer tank which is still pressurized and heated to prevent phase separation of the TMS system. At a lower temperature the solvent system would separate. This would inhibit the continuous transfer from the second buffer tank to the subsequent CSTR. Hence, the second buffer tank has to be considered as additional, small reaction zone in the detailed process optimization at miniplant conditions and with recycles. Following the CSTR, the reaction mixture is fed to downstream processing. The temperatures inside the SBR and CSTR are controlled by heating jackets and corresponding thermostats, whereas the two buffer vessels are heated by electrical heating tapes. The SBR+CSTR configuration is illustrated in Fig. 6 (a). The downstream and upstream buffer tanks require the same volume as the SBR to ensure same residence times. The reaction times in the SBR and the downstream buffer tank are summed up to the desired reaction time, corresponding to the residence time in the PFR designed before. Therefore, the SBR and the downstream buffer tank each have a volume of $V_R^{SBR} \approx 550$ ml.

4. Process Optimization

In order to assess the new reactor configurations, especially in comparison to the existing single CSTR setup, an optimization problem is developed that is based on the conditions in the miniplant. All of the previous optimizations in this work assume an ideal separation and recycle of pure substances such as introduced for the FPA in Section 2. In the following optimizations, a liquid-liquid phase separation in a decanter and a distillation column for product separation are included. The resulting flow sheet of the overall process is depicted in Fig. 7.

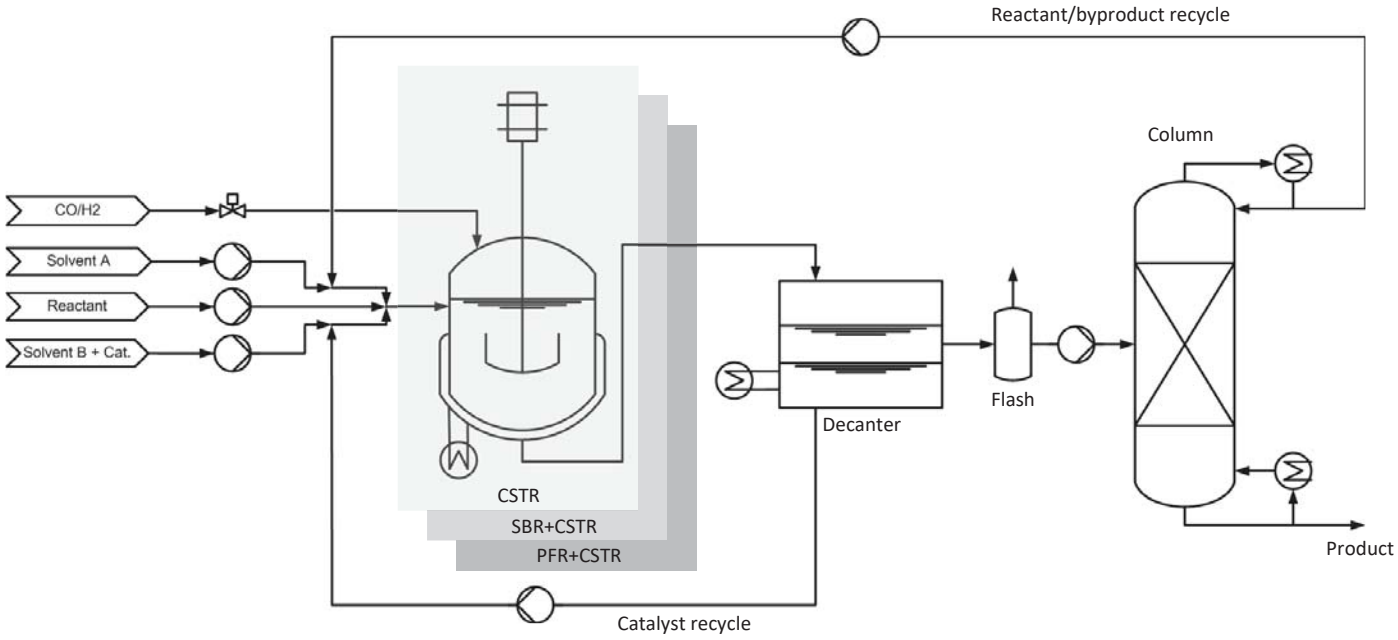

Figure 7: Overall process flow sheet used for optimization of the therein embedded optimized reactor concepts.

4.1 Modeling

4.1.1 Decanter

For determining the liquid-liquid phase equilibria (LLE) a Kriging model, introduced in McBride et al.[10], is considered. It uses a second order polynomial regression model with Gaussian correlation. As one can see from Eq. (4), the output variables $\hat{\theta}_{\alpha}^{polar}$ of the Kriging model, KR, are the molar fractions of n-,n-dimethylformamide, n-decane, 1-dodecene, tridecanal and Biphephos in the polar solvent phase. The input variables $\hat{x}_{\beta}$ are n-,n-dimethylformamide, n-decane and tridecanal. Note, that 2-methyldodecanal is added to the tridecanal fraction, n-dodecane to n-decane, and the iso-dodecenes to 1-dodecene for the input and output molar fractions. The latter can be calculated from the summation rule of the mole fractions to unity and is, thus, not given as particular input.

$$\hat{\theta}_{\alpha}^{polar} = KR\left(\hat{x}_{\beta}, T\right),$$

$$\alpha \in \{DMF, C10an, nC12en, nC13al, BPP\}$$

$$\beta \in \{DMF, C10an\ nC13al\} \quad (4)$$

The Kriging model is valid for temperatures between -25°C and $+25$°C. The resulting output streams of the decanter unit are calculated via Eqs. (5) – (6):

$$\dot{n}^{dec}_{\alpha,out,polar} = \hat{\theta}^{polar}_{\alpha} * \dot{n}^{dec}_{\alpha,in}\ ,\ \in \{CH, SOL\}\ , \quad (5)$$

$$\dot{n}^{dec}_{\alpha,out,apolar} = \left(1 - \hat{\theta}^{polar}_{\alpha}\right) * \dot{n}^{dec}_{\alpha,in}\ , \alpha \in \{CH, SOL\}. \quad (6)$$

4.1.2 Flash

The flash unit is only considered for pressure and gas release and not modeled in detail. Thus, the molar flow rates of the liquid components coming from the decanter are equal to the molar flow rates entering the distillation column:

$$\dot{n}^{dec}_{\alpha,out,apolar} = \dot{n}^{col}_{\alpha,in},\ \ \alpha \in \{CH, SOL\}. \quad (7)$$

4.1.3 Distillation Column

A short-cut model is embedded in the optimization for describing the distillation column. The Fenske-Underwood correlations are used to determine the composition of the distillate and bottom streams, and the number of trays. Since the products degrade at temperatures higher than 180°C, the distillation column is operated at vacuum pressure. For the sake of simplicity no pressure loss is considered. Aiming at a quantitative separation of the iso-dodecenes and the desired product tridecanal, the first is defined as light key (*LK*) and the latter as heavy key (*HK*) with split fractions of $\zeta^{D}_{LK} = 0.99$ and $\zeta^{D}_{HK} = 0.01$. For the calculation of relative volatilities with Eq. (A40), vapor pressure correlations are used given in Yaws[21] (see Eq. (A38)). For the iso-

dodecenes as well as the iso-aldehydes, fitted correlations from Hentschel et al.[9] are used (Eq. (A39)). The corresponding parameters for Eqs. (A38) – (A39) are provided in Tab. A5. A mean relative volatility is determined with Eq. (A41) and used for the calculation of the minimum number of stages with Eq. (A42). The resulting bottoms stream is finally computed by Eq. (8), whereby the distillate can be determined using the summation condition in Eq. (9).

$$\dot{n}_{\alpha}^{B} = \frac{\dot{n}_{\alpha,in}^{col}}{1+\frac{\zeta_{HK}^{D} * \dot{n}_{HK}^{in}}{\left(1-\zeta_{HK}^{D}\right) * \dot{n}_{HK}^{in}}} \tag{8}$$

$$\dot{n}_{\alpha,in}^{col} = \dot{n}_{\alpha}^{D} + \dot{n}_{\alpha}^{B} \tag{9}$$

4.2 Optimization Cases

The three process configurations to optimize are:

- Case 4.1: CSTR in overall process
- Case 4.2: SBR+CSTR in overall process
- Case 4.3: Helically coiled PFR+CSTR in overall process

Case 4.1 is depicted in Fig. 7. For cases 4.2 and 4.3 the reaction section (grey) in Fig. 7 is replaced by the optimized reactor concepts in Fig. 6 (a) and Fig. 6 (b), respectively. In all optimization cases the amount of reactant and solvents is kept constant using makeup-streams. This ensures that the mass fractions given in Tab. 1 are maintained in the reactor inlet. Based on these and the volumetric inlet flow rate given in Tab. 1, the predefined inlet molar streams are determined (Tab. 2).

Table 2: Predefined molar inlet streams for process optimization

Components	$\dot{n}_{\alpha}^{init}\ \left[\frac{\text{mol}}{\text{h}}\right]$
nC12en	0.1343
DMF	0.8116

C10an	0.4170

The volumetric flow rate at the inlet of the reaction section is limited to an upper value of $\dot{V}_{in,max}^{reactor} = 250\ \mathrm{ml/h}$. This value is close to the flow rate used in the experiments reported by Dreimann et al.[12], see Tab. 1, and allows one to investigate additional recycling potential.

- Case 4.1: The resulting optimization problem is given in the Appendix (DOP A1).
- Case 4.2: The SBR and the downstream buffer tank are modeled as one SBR with two control zones. The first zone, corresponding to the real SBR, can be dynamically controlled and acts completely in a discontinuous manner. The second zone, corresponding to the buffer tank, must have constant conditions. It is batch-wise filled from the SBR and feeds continuously to the CSTR. Thus, the latter stream is fluctuating. This fluctuation is handled by assuming a mean residence time in the buffer tank and feeding the corresponding mean composition to the CSTR. The optimization problem follows is stated in (DOP A2).
- Case 4.3: The modeling of the PFR (DSR) considers the spatial dimension z of the reactor and, thus, includes a flow velocity, see (DOP A3).

All dynamic optimization problems mentioned in this section, as well as the FPA in Section 2 and the reactor design study in Section 3, are discretized using orthogonal collocation, implemented as separate NLPs in AMPL and solved using the solver IPOPT 3.11.9 with the linear solver ma27. All solutions are local optima and, thus, depend on the initialization points which are mainly chosen by analysis of preliminary simulations of the process.

4.3 Results and Discussion

The three optimization cases reveal the performances of the existing miniplant reactor (single CSTR) and the two optimal reactor designs (see Fig. 6) operating with recycles from modeled separation units, replacing the

ideal separation assumed in Sections 2 and 3. The results are illustrated in Fig. 8. For an appropriate comparison, the S/X curves for the three cases are depicted as well, whereby the blue and green lines correspond to the blue and green lines in Fig. 5 (b), respectively. In contrast to Fig. 5, the depicted conversion range is very broad in order to allow for comparison with the existing CSTR performance to be made. Remember, the lines give the maximum performance before the detailed design is carried out. Thus, the size of the SBR and PFR are not fixed and the recycles are assumed to be ideally adjustable. As a result, the optimal performance of the CSTR and the two optimized reactor-networks are equal for small conversions. This is because the first reactor of both optimized reactor networks is neglected leading to a single CSTR configuration. Evidently, both optimized reactor-networks have a much higher selectivity potential for conversions higher than 0.4 than the single CSTR. This is caused by their longer residence times and the back-mixing benefit in the second reaction section.

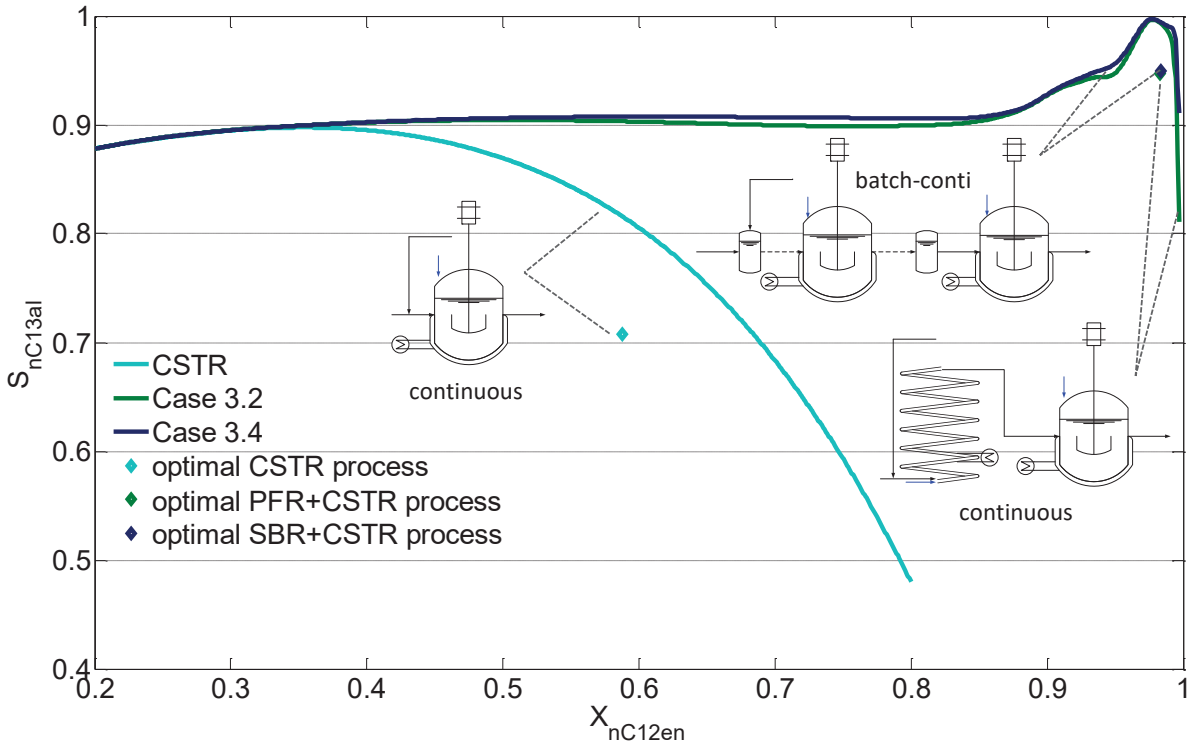

Figure 8: Comparison of performances of the existing (CSTR) and the two optimized reactor configurations (SBR+CSTR, PFR+CSTR) with real recycles, and with their corresponding maximum potentials

(corresponding color clines) under ideal recycle conditions and free dimensions of the first reactor for the optimized configurations (see Fig. 5).

The existing single CSTR configuration under real recycle conditions has its optimal selectivity of $S_{nC13al}^{opt} = 70.8\ \%$ at a conversion of $X_{nC13al}^{opt} = 58.8\ \%$, (the cyan diamond in Fig. 8). The higher selectivity potential in the regime of small conversions cannot be exploited because there the amount of beneficial iso-dodecenes recycled would decrease. Higher conversions, which would increase the iso-dodecene yield, cannot be achieved under the same conditions due to the limited residence time. The loss of the CSTR performance under real recycle conditions ($\Delta S \approx 11\ \%$.) is caused, on the one hand, by the recycle of aldehydes in the polar solvent recycled from the decanter, and on the other hand, by the recycle of useless n-dodecane from the column distillate. If, instead, more iso-dodecenes could be recycled, it would be beneficial. Consequently, the purge of the column recycle is set to $\xi_{rec}^{col} = 37\ \%$ in order to reduce the amount of n-dodecane recycled at the expense of the reduced iso-dodecene recycle, and to enable the optimal ratio of iso-dodecenes to 1-dodecene in the reactor inlet. The compositions of the streams in the corresponding overall process are illustrated in Fig. 9 (a).

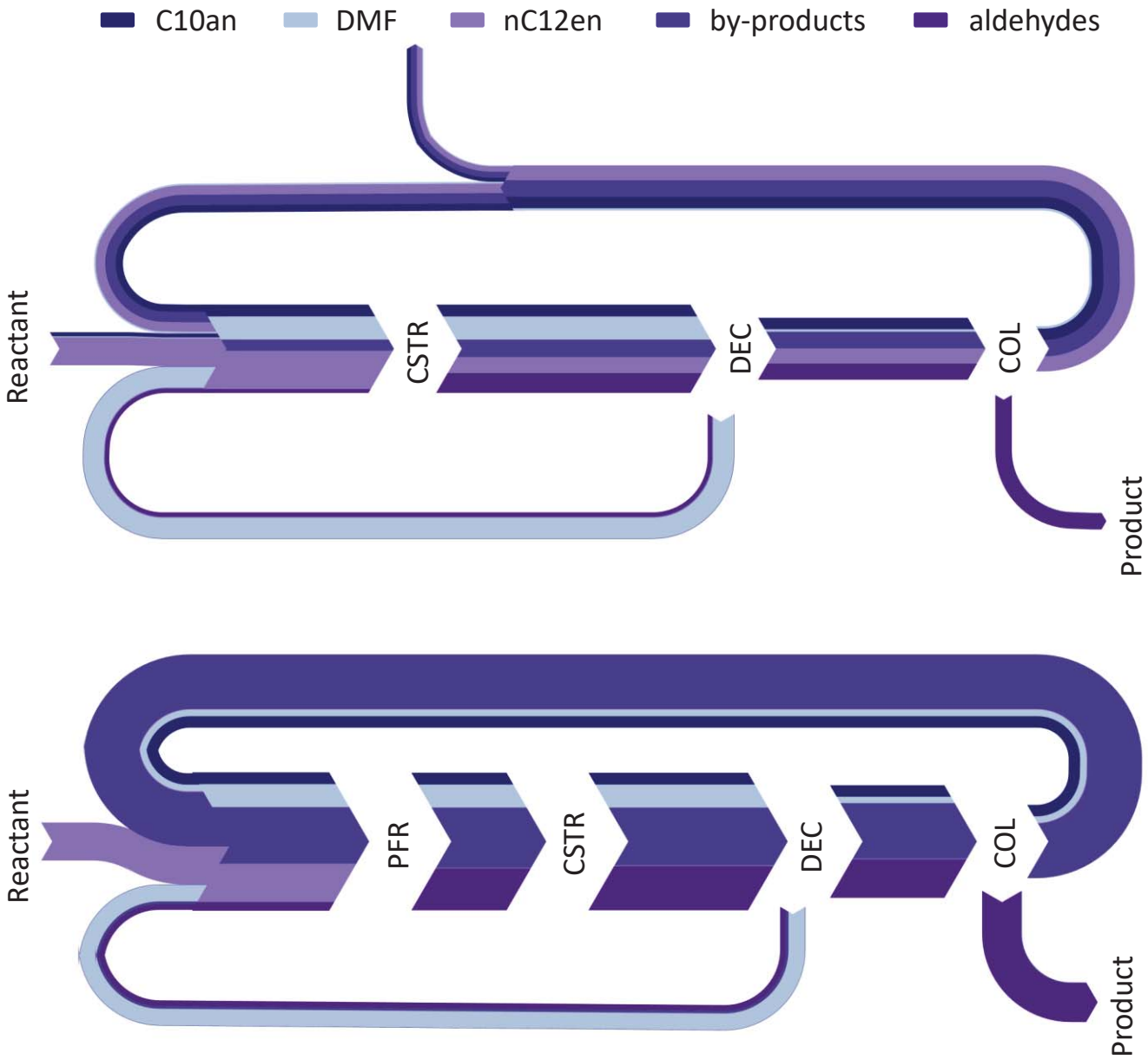

Figure 9: Sankey flow diagrams for (a) the CSTR embedded in the overall process and (b) the optimized PFR+CSTR configuration embedded in the overall process. Note, that the mass streams of the solvents (C10an, DMF) are downsized by a factor of 10 to allow for a better illustration.

The batch-conti realization in the optimized SBR+CSTR network has its optimal selectivity of $S_{nC13al}^{opt} =$ 94.9 % at a conversion of $X_{nC13al}^{opt} = 98.3$ %, (the blue diamond in Fig. 8). The optimal conversion is close to the estimated optimal conversion point from the reactor design study in Section 3. Although the dynamic

control is limited to only the first half of the reaction time of the SBR, due to the consideration of reaction time in the buffer tank, the extension of the CSTR with an upstream SBR leads to a significant increase in both the selectivity and conversion. Due to the different reaction conditions, the n-dodecane in the distillate recycle is useful and desirable in the reactor feed. Its presence leads to less n-dodecane formation from the reactant, since they are closer to chemical equilibrium (comparable to advantage of iso-dodecene recycle, see Fig. 2). Thus, the purge of the column distillate recycle can be set to $\xi_{rec}^{col} = 0$ % and no reactant and byproduct is wasted. Aldehydes are not recycled. The loss of selectivity in comparison to the case of ideal recycle is at $\Delta S \approx 4$ %.

The optimal continuous reactor-network consisting of the helically coiled tube reactor and the CSTR has its optimal selectivity of $S_{nC13al}^{opt} = 94.7$ % at a conversion of $X_{nC13al}^{opt} = 98.3$ %, (the green diamond in Fig. 8). Since the conversion and the residence times are equal, the same reasoning for the performance enhancement and recycling benefit holds as for the SBR+CSTR network. The small difference in selectivity might arise from the reduced gas phase control in the helically coiled tube reactor. Again, no purge of distillate recycle is necessary $\xi_{rec}^{col} = 0$ % and the loss by real separation is at $\Delta S \approx 4$ %. Note, when considering pressure drop in the tube due to the consumption of the gas phase by the chemical reaction, the gas and liquid phase volume will change along the reactor length. For a defined residence time this will certainly lead to a reduction of the reactor length.

The clear advantage of the improved reactor design becomes further obvious when analyzing the compositions of the streams in the corresponding overall process (Fig. 9 (b)). One can see that due to the higher conversion much less reactant is recycled instead higher amounts of byproducts. This improves the process performance as shown in the FPA in Section 2. The stream compositions of the SBR+CSTR configuration are very similar to the ones depicted in Fig. 9 (b).

The stream compositions in both cases show impressively how the solvents are recycled as two phases. The DMF containing the catalyst is recycled together with aldehydes from the decanter unit (DEC), and the n-decane is recycled together with the remaining reactant and the byproducts from the distillation column (COL).

5. Conclusion

For the hydroformylation of 1-dodecene using a rhodium catalyst and a thermomorphic solvent system for catalyst recovery, the design for a miniplant-scale reactor is successfully carried out based on predictions from dynamic optimizations. For identification of promising reactor-networks, the *Flux Profile Analysis* introduced in Kaiser et al.[13] is applied to this challenging, multiphase process. It turns out to be a powerful tool revealing the advantages of different reactor-network candidates. From those candidates suitable for the hydroformylation process, the configuration of a distributed sidestream reactor with initial product dosing and a subsequent back-mixed CSTR seems to be most reasonable for technical realization. The design of this reactor-network for an existing miniplant produces two promising realization options: (i) a continuous flow reactor followed by a CSTR and (ii) a discontinuously operated semibatch reactor followed by a CSTR. The first option shows to be sufficiently approximated by a PFR and CSTR, including individual dosing of gaseous reactants to both reactors. The second option is more challenging the technical realization due to the combination of batch and continuous reactors, but allows for a very accurate realization of dynamic control actions. Both reactors are designed for the conditions of the miniplant, whereby the second reactor in each case (CSTR) is considered to be the already existing CSTR currently used in the miniplant (see. Dreimann et al.[11,12]). The different operational modes within the SBR+CSTR network and the overall process are merged by using buffer tanks before and after the SBR. The PFR in the first realization is designed as a helically coiled tube reactor providing a beneficial intermittent flow with high mass transfer rates and low axial dispersion. Both designs are embedded in an overall process optimization considering both a liquid-liquid phase separation for solvent and catalyst recovery and a distillation column for product separation and reactant/byproduct recycling. The performance regarding selectivity w.r.t. the desired aldehyde and the conversion is drastically increased by the two optimized reactor designs. Both have an optimal selectivity around 95 % at a conversion around 98 % which indicates an enhancement of 24 % and 40 % in comparison to the existing CSTR, respectively. The comparison of the existing CSTR and both optimal reactor-networks to the case of ideal recycling reveals the loss by technical approximation and non-ideal separations.

This work shows how the application of model-based reactor-network synthesis can support and enhance the reactor design for a miniplant-scale experimental setup. The experimental investigation of the actual impact of recycling on the reactor performance will further advance the establishment of a hydroformylation process for long-chain olefins using thermomorphic solvent systems for industrial application.

Associated Content:

A.1 Model equations, kinetics, thermodynamic relations, and all corresponding parameters:

Balance equations for the batch reactor in the *Flux Profile Analysis*

$$\frac{dn_\alpha}{dt} = \left(\sum_{m=1}^{M} \nu_{\alpha,m} r_m\right) V_{liq} c_{cat} M_{cat} + j_\alpha(t),\ \alpha \in CH, \tag{A1}$$

and those for the storage tanks are

$$\frac{dn_{a,st}}{dt} = -j_a(t),\ \alpha \in CH\ , \tag{A2}$$

where $\boldsymbol{n} \in \mathbb{R}^N$ are the molar reactor holdups; $\boldsymbol{j} \in \mathbb{R}^N$ are the dosing streams; $\boldsymbol{r} \in \mathbb{R}^M$ are the reaction rates with $\boldsymbol{r} = \boldsymbol{r}(\boldsymbol{c}, T)$ being a function of the component concentrations $\boldsymbol{c}$ and the temperature T; $\nu_{\alpha,m}$ are the stoichiometric coefficients; and V_{liq} is the liquid reaction volume; c_{cat} is the active catalyst concentration and M_{cat} is its molar mass. The reaction rates (Eqs. (A3) - (A9)) were determined in Kiedorf et al.[7] and refined in Hentschel et al.[8]. The solvent system and the catalyst used are identical to the system described in Section 1.

$$r_1 = \frac{k_{1,0}(T) c_{nC12en} c_{H2} c_{CO}}{1 + K_{1,1} c_{nC12en} + K_{1,2} c_{nC13al} + K_{1,3} c_{H2}} \tag{A3}$$

$$r_2 = \frac{k_{2,0}(T)\left(c_{nC12en} - \frac{c_{iC12en}}{K_{eq,2}}\right)}{1 + K_{2,1} c_{nC12en} + K_{2,2} c_{iC12en}} \tag{A4}$$

$$r_3 = \frac{k_{3,0}(T)\left(c_{nC12en} c_{H2} - \frac{c_{nC12an}}{K_{eq,3}}\right)}{1 + K_{3,1} c_{nC12en} + K_{3,2} c_{nC12an} + K_{3,3} c_{H2}} \tag{A5}$$

$$r_4 = k_{4,0}(T) c_{iC12en} c_{H2} \tag{A6}$$

$$r_5 = k_{5,0}(T) c_{iC12en} c_{H2} c_{CO} \tag{A7}$$

$$r_6 = k_{6,0}(T) c_{nC12en} c_{H2} c_{CO} \tag{A8}$$

$$c_{cat} = \frac{c_{cat,tot}}{1 + K_{cat,1} c_{CO}^{K_{cat,3}} + K_{cat,2} \frac{c_{CO}^{K_{cat,3}}}{c_{H2}}} \tag{A9}$$

The temperature dependencies of the reaction constants $k_{j,0}$ are modeled via an Arrhenius equation

$$k_j(T) = k_{0,j}\, exp\left(\frac{-E_{A,j}}{R}\left(\frac{1}{T} - \frac{1}{T_{ref}}\right)\right) \quad , j \in RCT\ , \tag{A10}$$

with $T_{ref} = 378.15\ K$. The equilibrium constants $K_{p,j}$ are calculated via

$$K_{p,j} = exp\left(\frac{-\Delta_R G_j}{RT}\right), \tag{A11}$$

$$\Delta_R G_j = a_{0,j} + a_{1,j} T + a_{2,j} T^2,\ j \in \{2,3\}. \tag{A12}$$

The parameters for rate equations and reaction constants are given in Tab. A1 and A2.

The batch reactor is assumed to be ideally mixed and its liquid volume and required densities are calculated using Eqs. (A13) – (A14), respectively. The corresponding parameters can be found in Tab. A3.

$$V_{liq} = \sum_{\alpha \in COM} \frac{n_\alpha^{liq} M_\alpha}{\rho_\alpha} \tag{A13}$$

$$\rho_\alpha = a_{\rho,0,\alpha} + a_{\rho,1,\alpha} T \tag{A14}$$

The concentrations of the dissolved gases in the liquid phase are equal to their maximal solubilities, which are calculated with their partial pressures and Henry coefficients expressed using an exponential expression for temperature dependency.

$$c_\alpha^* = \frac{p_\alpha}{H_\alpha} \quad , \alpha \in \{GAS\} \tag{A15}$$

$$H_\alpha = H_\alpha^0 exp\left(\frac{-E_{A,H_\alpha}}{RT}\right) \quad \text{(A16)}$$

The parameters used in Eq. (A16) have been previously fitted to the reaction system[8] and are given Tab. A4.

In addition to the balance equations, reaction kinetics, and thermodynamic properties, certain constraints on reactant use (Eq. (A17)) and product dosing (Eq. (A18)) need to be satisfied[13]:

$$\int_0^{t_f} j_\alpha(t)\, dt \geq n_\alpha^{min}, \alpha \in \{reactants\}\,, \quad \text{(A17)}$$

$$\int_0^{t_f} j_\alpha(t)\, dt + n_{\alpha,st}(t_f) = n_{\alpha,st}(t=0),\ \alpha \in \{prod.\}\,. \quad \text{(A18)}$$

Table A1: Parameters for rate equations and catalyst equilibrium (Eqs. (A3)-(A9))

Variable	Eq.	$E_A\left[\frac{kJ}{mol}\right]$	k_0	Unit	$K_1\left[\frac{ml}{mol}\right]$	$K_2\left[\frac{ml}{mol}\right]$	$K_3\left[\frac{ml}{mol}\right]$
r_1	(A3)	113.08	4.904e16	$\frac{ml^3}{g\,min\,mol^2}$	574876	3020413	11732838
r_2	(A4)	136.89	4.878e6	$\frac{ml}{g\,min}$	38632	223214	-
r_3	(A5)	76.11	2.724e8	$\frac{ml^2}{g\,min\,mol}$	2661.2	7100	1280
r_4	(A6)	102.26	2.958e4	$\frac{ml^2}{g\,min\,mol}$	-	-	-
r_5	(A7)	120.84	3.702e10	$\frac{ml^3}{g\,min\,mol^2}$	-	-	-
r_6	(A8)	113.08	3.951e11	$\frac{ml^3}{g\,min\,mol^2}$	-	-	-
c_{cat}	(A9)	-	-	-	3.041e4	0	0.644

Table A2: Parameters for equilibrium constants (Eq.(A12))

Variable	$a_0 \left[\frac{kJ}{mol}\right]$	$a_1 \left[\frac{kJ}{mol\ K}\right]$	$a_2 \left[\frac{kJ}{mol\ K^2}\right]$
ΔG_2	-11.0034	0	0
ΔG_3	-126.275	0.1266	6.803e-6

Table A3: Parameters for density correlation (Eq. A14)

Component	$a_0 \left[\frac{kg}{m^3}\right]$	$a_1 \left[\frac{kg}{m^3 K}\right]$
C10an	981.60	-8.3536e-1
DMF	1256.52	-1.0306
nC12en	993.89	-7.8875e-1
nC12an	977.04	-7.6743e-1
nC13al	1068.12	-8.0180e-1
iC12en	993.89	-7.8875e-1
iC13al	1068.12	-8.0180e-1

Table A4: Parameters for the solubility coefficient calculation in Eq. (A16).

Component	$H_0 \left[\frac{bar\ ml}{mol}\right]$	$E_{A,H} \left[\frac{kJ}{mol}\right]$
H_2	66400	-3.06

CO	73900	-0.84

Table A5: Parameters for vapour pressure calculation in Eqs. (A38) – (A39).

Component	a_0	a_1	a_2	a_3	a_4
C10an	-26.51	-3.358e3	-6.117	-3.323e-10	4.855e-7
DMF	47.99	-2.385e3	28.80	-5.860e-2	3.139e-5
nC12en	-8.59	-3.524e3	10.81	-2.816e-2	1.427e-5
nC12an	-5.653	-3.470e3	9.027	-2.319e-2	1.124e-5
nC13al	161.5	-9.766e3	-55.59	2.104e-2	5.550e-13
iC12en	75.79	-9.964e3	-8.965	4.940e-18	6
iC13al	10.42	-6.149e3	0.197	-2e-4	1

A.2 Balance equations:

- Plug Flow Reactor (PFR):

$$\frac{d\dot{n}_\alpha^{liq}}{dz} = \left(\sum_{m=1}^{M} \nu_{\alpha,m} r_m\right) V_{liq} v_s^{-1} c_{cat} M_{cat},\ \alpha \in \{CH\} \qquad \text{with } \dot{n}_\alpha^{liq}(z=0) = \dot{n}_{\alpha,0}^{liq}, \tag{A19}$$

$$\frac{d\dot{n}_\alpha^{liq}}{dz} = k_L a\, V_{liq} v_s^{-1}\left(c_\alpha^* - c_\alpha^{liq}\right) + \left(\sum_{m=1}^{M} \nu_{\alpha,m} r_m\right) V_{liq} v_s^{-1} c_{cat} M_{cat},\ \alpha \in \{GAS\} \qquad \text{with } \dot{n}_\alpha^{liq}(z=0) = \dot{n}_{\alpha,0}^{liq}, \tag{A20}$$

$$\frac{d\dot{n}_{\alpha}^{gas}}{dz} = -k_L a\, V_{liq} v_s^{-1}\left(c_{\alpha}^{*} - c_{\alpha}^{liq}\right),\ \alpha \in \{GAS\} \qquad \text{with } \dot{n}_{\alpha}^{gas}(z=0) = \dot{n}_{\alpha,0}^{gas}\,,$$

(A21)

$$\dot{n}_{\alpha,0}^{liq} = \dot{n}_{\alpha}^{makeup} + \dot{n}_{\alpha}^{rec,dec} + \dot{n}_{\alpha}^{rec,col}, \alpha \in \{CH, SOL\}$$

(A22)

$$\dot{n}_{\alpha,0}^{liq} = 0\,, \alpha \in \{GAS\}$$

(A23)

$$\dot{n}_{\alpha,0}^{gas} = j_{\alpha}^{gas}, \alpha \in \{GAS\}$$

(A24)

- Distributed Sidestream Reactor (DSR):

The balance equations and initial conditions for the PFR are extended by replacing Eq. (A21) with Eq. (A25). Thus, the only difference is the distributed dosing of gaseous reactants H_2 and CO.

$$\frac{d\dot{n}_{\alpha}^{gas}}{dz} = j_{\alpha}^{gas} - k_L a\, V_{liq} v_s^{-1}\left(c_{\alpha}^{*} - c_{\alpha}^{liq}\right),\ \alpha \in \{GAS\} \quad \text{with } \dot{n}_{\alpha}^{gas}(z=0) = \dot{n}_{\alpha,0}^{gas}\,,$$

(A25)

- Semibatch Reactor (SBR):

$$\frac{dn_{\alpha}^{liq}}{dt} = \left(\sum_{m=1}^{M} \nu_{\alpha,m} r_m\right) V_{liq} c_{cat} M_{cat},\ \alpha \in \{CH\} \quad \text{with } n_{\alpha}^{liq}(t=0) = n_{\alpha,0}^{liq}\,,$$

(A26)

$$\frac{dn_{\alpha}^{liq}}{dt} = k_L a\, V_{liq}\left(c_{\alpha}^{*} - c_{\alpha}^{liq}\right) + \left(\sum_{m=1}^{M} \nu_{\alpha,m} r_m\right) V_{liq} c_{cat} M_{cat},\ \alpha \in \{GAS\} \qquad \text{with } n_{\alpha}^{liq}(t=0) = n_{\alpha,0}^{liq}\,,$$

(A27)

$$\frac{dn_{\alpha}^{gas}}{dt} = j_{\alpha}^{gas} - k_L a\, V_{liq}\left(c_{\alpha}^{*} - c_{\alpha}^{liq}\right),\ \alpha \in \{GAS\} \quad \text{with } n_{\alpha}^{gas}(t=0) = n_{\alpha,0}^{gas}\,,$$

(A28)

$$n_{\alpha,0}^{liq} = \dot{n}_{\alpha}^{makeup} t_{SBR} + \dot{n}_{\alpha}^{rec,dec} t_{SBR} + \dot{n}_{\alpha}^{rec,col} t_{SBR}, \alpha \in \{CH, SOL\}$$

(A29)

$$n_{\alpha,0}^{liq} = 0\,, \alpha \in \{GAS\}$$

(A30)

$$n_{\alpha,0}^{gas} = 0, \alpha \in \{GAS\}$$

(A31)

- Continuous Stirred Tank Reactor (CSTR):

$$0 = \dot{n}_{\alpha}^{liq} - \dot{n}_{\alpha,0}^{liq} + \left(\sum_{m=1}^{M} \nu_{\alpha,m} r_m\right) V_{liq} c_{cat} M_{cat}, \quad \alpha \in \{CH\}$$

(A32)

$$0 = \dot{n}_{\alpha}^{liq} + \left(\sum_{m=1}^{M} \nu_{\alpha,m} r_m\right) V_{liq} c_{cat} M_{cat} + k_L a\, V_{liq}\left(c_{\alpha}^{*} - c_{\alpha}^{liq}\right), \quad \alpha \in \{GAS\}$$

(A33)

$$0 = \dot{n}_{\alpha}^{gas} - k_L a\, V_{liq}\left(c_{\alpha}^{*} - c_{\alpha}^{liq}\right), \quad \alpha \in \{GAS\}$$

(A34)

A.3 Details of reactor design and preliminary experiments:

With the previously estimated flow rate, the restriction to a liquid hold-up of $\varepsilon_{liq} = 0.33$ and the tube diameter limitation of $1\ \text{mm} \leq d \leq 10\ \text{mm}$, the resulting superficial velocity for the liquid and gas phase is in the range $7.08\ 10^{-4}\ \text{m/s} \leq v_s \leq 0.0707\ \text{m/s}$.

Albeit the literature results already suggest the correct flow pattern for the given conditions, they are carried out for species with different surface tensions and for higher superficial velocities. To ensure the formation of the desired flow pattern for the used solvent system and flow rates, experiments are carried out under the conditions of the miniplant.

The experimental setup consists of a helically coiled tube made of silicon, PFA or PTFE, to enable visual observation of the flow patterns, with diameters of $d_{tube} = 1.6\ \text{mm}, 2.0\ \text{mm}$ and $3.0\ \text{mm}$ and a length between $2\ \text{m} \leq l \leq 6\ \text{m}$. The coils have a diameter of $d_{coil} = 10\ \text{cm}$ and are coiled around a yellow PVC cylinder. The liquid phase is fed to the helically coiled tube by a pump (Smartline 1050, KNAUER Wissenschaftliche Geräte GmbH) and the gas phase is fed using a rotameter (DK800, Krohne Messtechnik GmbH). For determining the pressure loss two pressure transducers (CPT6200, Wika Alexander Wiegand SE & Co. KG) are installed at the tube inlet and outlet. The pressure inside the tube is maintained on a level which ensures the desired liquid hold-up of $\varepsilon_{liq}^{PFR} = 0.33$. This is managed using a needle valve at the outlet and the measurements obtained by the transducers. A scheme of the setup is shown in Fig. A2.

To simplify handling, the flow investigation experiments were carried out with the substitute species 2-propanol which has a lower surface tension than the original solvent system (DMF, n-decane). Thus, if the desired intermittent flow regime is stable for 2-propanol, it will a fortiori be stable for the original solvent system. The synthesis gas was replaced with air.

Preliminary studies about the characteristic flow patterns of a helically coiled tube have shown that for low volumetric flow rates a horizontal orientation suffers more from gravitational forces than a vertical orientation. Furthermore, it was observed that a tube diameter larger than $6\ mm$ no longer allows for an intermitted flow regime.

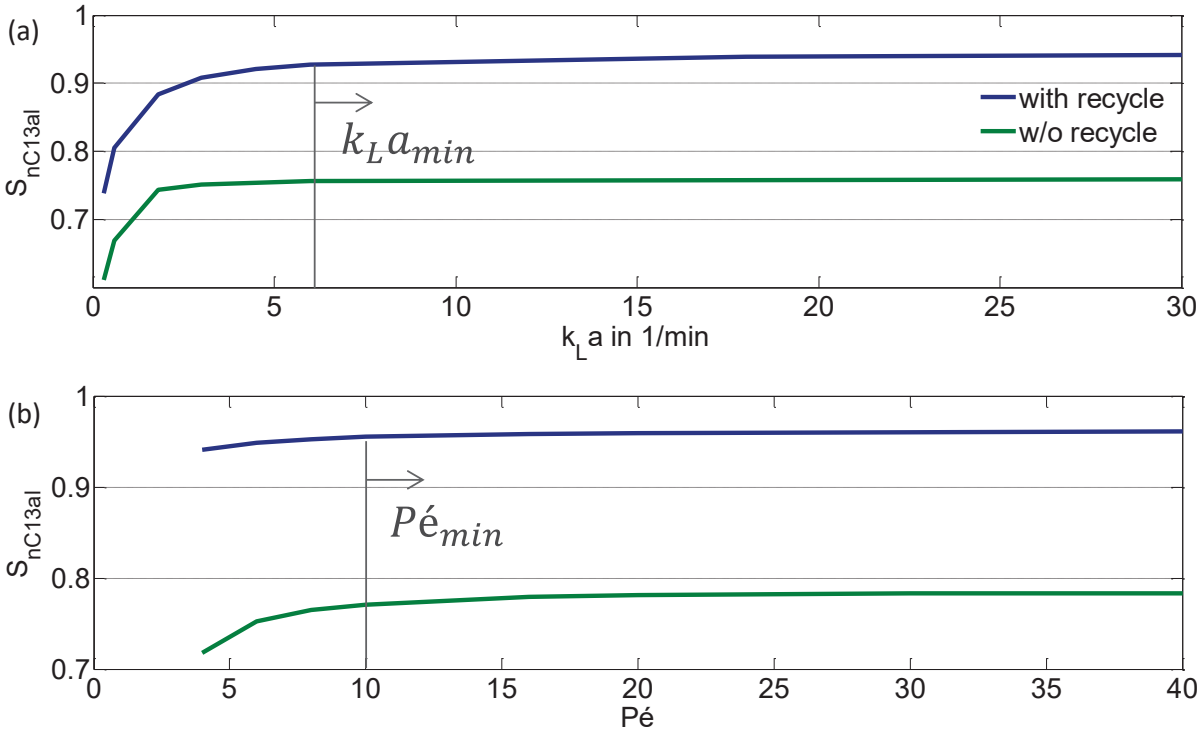

Figure A1: Selectivity w.r.t. tridecanal (nC13al) over the $\boldsymbol{k_L a}$ value (a) and the ***P***é number (b) for the case of product recycling (blue) and no product recycling (green).

The experimental results are visualized in Fig. A3. It can be seen that for all tube diameters and volumetric liquid flow rates intermittent flow is maintained. The volumetric flow rate of $\dot{V}_{liq}^{in} \approx 200$ ml/h is chosen as an upper limit. For a tube diameter of $d_{tube} = 3$ mm a slight decomposition into a stratified flow and re-composition to an intermittent flow was observed, but only for the lowest flow rate. As expected, the pressure loss $\Delta p/l$ increases with decreasing tube diameter and increasing volumetric flow rate. Thus, a trade-off has to be found between a small tube diameter, which ensures intermittent flow but leads to a longer tube, and small pressure drop. The appropriate tube diameter was chosen to be $d_{tube} = 3$ mm due to the stable intermittent flow regime at a volumetric flow rate of $\dot{V}_{liq}^{in} \approx 200$ ml/h and the acceptable pressure drop observed. The pressure drop for smaller tube diameters was significantly higher reducing their effectiveness. This leads to a final reactor length of $l_{PFR} \approx 311$ m. Taking the experimentally determined pressure drop from Fig. A3 into account, the reactor has a pressure drop of $\Delta p = 0.5287$ bar caused by flow induced friction.

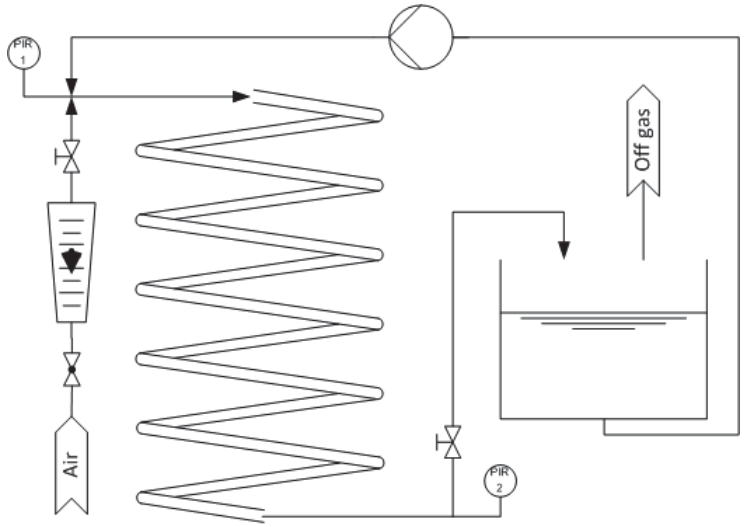

Figure A2: Scheme of the experimental setup consisting of a helically coiled tube of different radii and storage tank for the mixture of water and 2-propanol; air is dosed via rotameter to the helix and liquid phase via pump from the storage tank; pressure transducers at the inlet and outlet for pressure drop registration.

$\dot{V}_{liq}$ \ d	1.6 mm	2.0 mm	3.0 mm
$1.1\frac{ml}{min}$	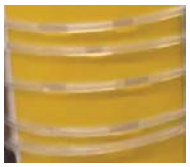 $\frac{\Delta p}{l} = 0.0025\ \frac{bar}{m}$	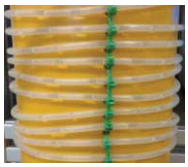 $\frac{\Delta p}{l} = 0.0011\ \frac{bar}{m}$	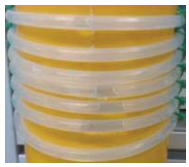 $\frac{\Delta p}{l} = 0.0010\ \frac{bar}{m}$
$1.7\frac{ml}{min}$	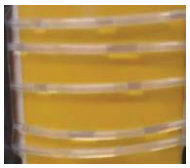 $\frac{\Delta p}{l} = 0.0035\ \frac{bar}{m}$	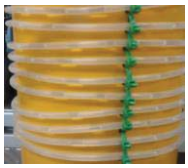 $\frac{\Delta p}{l} = 0.0017\ \frac{bar}{m}$	 $\frac{\Delta p}{l} = 0.0010\ \frac{bar}{m}$
$3.3\frac{ml}{min}$	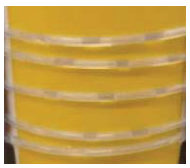 $\frac{\Delta p}{l} = 0.0060\ \frac{bar}{m}$	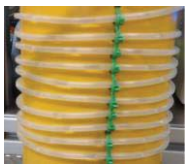 $\frac{\Delta p}{l} = 0.0043\ \frac{bar}{m}$	 $\frac{\Delta p}{l} = 0.0017\ \frac{bar}{m}$

Figure A3: Photographs of the flow regimes within the test setup (Fig. A2) for different flow regimes $\dot{\boldsymbol{V}}_{\boldsymbol{liquid}}$ and tube diameters $\boldsymbol{d}$; the transparent tubes are coiled around the yellow PVC cylinder and fixed with the green cable tie.

A.4 Additional flow sheet equations:

$$\dot{n}_{\alpha}^{makeup} = \dot{n}_{\alpha}^{init}, \alpha \in \{nC12en, C10an, DMF\} \tag{A35}$$

$$\dot{n}_{\alpha}^{rec,dec} = \dot{n}_{\alpha,out,apolar}^{dec}\, \xi_{rec}^{dec}, \alpha \in \{CH, SOL\} \tag{A36}$$

$$\dot{n}_{\alpha}^{rec,col} = \dot{n}_{\alpha,out,apolar}^{col}\, \xi_{rec}^{col}, \alpha \in \{CH, SOL\} \tag{A37}$$

A.5 Vapor pressures, volatilities, and minimum tray number for distillation column:

$$p_{\alpha}^{vap} = 10\left(a_0 + \frac{a_1}{T} + a_2 \log_{10}(T) + a_3 T + a_4 T^2\right) * 133.322e-6,$$

$$\alpha \in \{nC12en, nC13al, nC12an, DMF, C10an\} \tag{A38}$$

$$p_{\alpha}^{vap} = exp\left(a_0 + \frac{a_1}{T} + a_2 \ln(T) + a_3 T^{a_4}\right) * 0.1, \quad \alpha \in \{iC12en, iC13al\} \tag{A39}$$

$$\kappa_{\alpha,\beta} = \frac{p_{\alpha}^{vap}(T)}{p_{\beta}^{vap}(T)} \tag{A40}$$

$$\bar{\kappa}_{\alpha,\beta} = \sqrt{\kappa_{\alpha,\beta}(T_D) * \kappa_{\alpha,\beta}(T_B)} \tag{A41}$$

$$N_{min} = \frac{\log\left(\frac{\dot{n}_{LK}^{D} \dot{n}_{HK}^{B}}{\dot{n}_{LK}^{B} \dot{n}_{HK}^{D}}\right)}{\log(\bar{\kappa}_{LK,HK})} \tag{A42}$$

A.6 Reactor indices:

$$S_{nC13al} = \frac{\dot{n}^f_{nC13al} - \dot{n}^0_{nC13al}}{\dot{n}^0_{nC12en} - \dot{n}^f_{nC12en}} \quad \text{(A43)}$$

$$X_{nC12en} = \frac{\dot{n}^0_{nC12en} - \dot{n}^f_{nC12en}}{\dot{n}^0_{nC12en}} \quad \text{(A44)}$$

$$STY_{nC13al} = \frac{\dot{n}^f_{nC13al}}{V_{reactor}} \quad \text{(A45)}$$

$$n/iso = \frac{\dot{n}^f_{nC13al}}{\dot{n}^f_{nC13al} + \dot{n}^f_{iC13al}} \quad \text{(A46)}$$

A. 7 Dynamic Optimization Problems:

$$\max_{u,p} \{S_{nC13al}(t_f)\} \quad \text{(DOP A1)}$$

s.t. Reactor mass balances: Eq. (A32) – (A34)

Reaction kinetics: Eqs. (A3) – (A12)

Constitutive equations: Eqs. (A13) – (A14)

Gas solubilities: Eqs. (A15) – (A16)

Decanter: Eqs. (4) – (6)

Flash: Eq. (7)

Distillation column: Eqs. (A38) – (A42), Eqs. (8) – (9)

Flow sheet: Eqs. (A35) – (A37)

Purges: $\xi^{dec}_{rec} = 1, 1 \geq \xi^{col}_{rec} \geq 0,$

Initial conditions: Eq. (A4) – (A6), Tab. 2

Reactor indices: Eqs. (A25) – (A28), $n/iso\ ratio \geq 95\%,$

Stream constraints: $j_{CO}, j_{H_2} \geq 0, \dot{n}_\alpha(t) \geq 0,$

Pressure: $10\ \text{bar} \leq p^{CSTR}_{total} = p^{CSTR}_{CO} + p^{CSTR}_{H_2} \leq 21\ \text{bar},$

Temperature: $363.15\ \text{K} \leq T_{CSTR} \leq 388.15\ \text{K},$

Reactor volume: $V_{CSTR} \leq 1\,\mathrm{l}, \varepsilon_{liq}^{CSTR} = 0.3,$

Controls: $u = \left[T_{CSTR}, j_{CO}, j_{H_2}\right], p = [\xi_{rec}^{dec}, \xi_{rec}^{col}].$

$$\max_{u(t),p} \left\{S_{nC13al}\left(t_f\right)\right\} \qquad \text{(DOP A2)}$$

s.t. Reactor mass balances: Eq. (A26) – (A28), Eq. (A32) – (A34)

Reaction kinetics: Eqs. (A3) – (A12)

Constitutive equations: Eqs. (A13) – (A14)

Gas solubilities: Eqs. (A15) – (A16)

Decanter: Eqs. (4) – (6)

Flash: Eq. (7)

Distillation column: Eqs. (A38) – (A42), Eqs. (8) – (9)

Flow sheet: Eqs. (A35) – (A37)

Purges: $\xi_{rec}^{dec} = 1,\ 1 \geq \xi_{rec}^{col} \geq 0$

Initial conditions: Eqs. (A11) – (A13), Tab. 2

Reactor indices: Eqs. (A25) – (A28), $n/iso\ ratio \geq 95\%,$

Stream constraints: $j_{CO}^{SBR}(t), j_{H_2}^{SBR}(t), j_{CO}^{CSTR}, j_{H_2}^{CSTR} \geq 0, \dot{n}_{\alpha}(t) \geq 0,$

Pressure: $10\ \mathrm{bar} \leq p_{total}^{CSTR} = p_{CO}^{CSTR} + p_{H_2}^{CSTR} \leq 21\ \mathrm{bar},$

$$10\ \mathrm{bar} \leq p_{total}^{SBR}(t) = p_{CO}^{SBR}(t) + p_{H_2}^{SBR}(t) \leq 21\ \mathrm{bar},$$

$$p_{CO}^{SBR}(t) = const.\, for\ t \geq \frac{t_{SBR}}{2},$$

$$p_{H_2}^{SBR}(t) = const.\, for\ t \geq \frac{t_{SBR}}{2},$$

Temperature: $363.15\ \mathrm{K} \leq T_{CSTR} \leq 388.15\ \mathrm{K},$

$$363.15\ \mathrm{K} \leq T_{SBR}(t) \leq 388.15\ \mathrm{K},$$

$$T_{SBR}(t) = const.\, for\ t \geq \frac{t_{SBR}}{2},$$

Reactor volume: $V_{CSTR} \leq 1\,\mathrm{l}, \varepsilon_{liq}^{CSTR} = 0.3, V_{SBR} = 1.1\,\mathrm{l}, \varepsilon_{liq}^{SBR} = 0.66,$

Controls: $u(t) = \left[T_{SBR}(t), j_{CO}^{SBR}(t), j_{H_2}^{SBR}(t)\right],$

$p = [T_{CSTR}, j_{CO}^{CSTR}, j_{H_2}^{CSTR}, \xi_{rec}^{dec}, \xi_{rec}^{col}],$

Buffer tank: $\dot{n}_{\alpha,in}^{CSTR} = 1/(\frac{t_{SBR}}{2}) \int_{t_{SBR}/2}^{t_{SBR}} \dot{n}_{\alpha}^{SBR}.$

$$\max_{u(z),p} \left\{S_{nC13al}(\tau_f)\right\} \qquad \text{(DOP A3)}$$

s.t. Reactor mass balances: Eq. (A19) – (A21), Eq. (A32) – (A34)

Reaction kinetics: Eqs. (A3) – (A12)

Constitutive equations: Eqs. (A13) – (A14)

Gas solubilities: Eqs. (A15) – (A16)

Decanter: Eqs. (4) – (6)

Flash: Eq. (7)

Distillation column: Eqs. (A38) – (A42), Eqs. (8) – (9)

Flow sheet: Eqs. (A35) – (A37)

Purges: $\xi_{rec}^{dec} = 1, 1 \geq \xi_{rec}^{col} \geq 0,$

Initial conditions: Eqs. (A11) – (A13), Tab. 2

Reactor indices: Eqs. (A25) – (A28), $n/iso\ ratio \geq 95\%,$

Stream constraints: $j_{CO}^{PFR}(z), j_{H_2}^{PFR}(z), j_{CO}^{CSTR}, j_{H_2}^{CSTR} \geq 0, \dot{n}_{\alpha}(z) \geq 0, \dot{n}_{\alpha}(z) \geq 0,$

Pressure: $10\ \mathrm{bar} \leq p_{total}^{CSTR} = p_{CO}^{CSTR} + p_{H_2}^{CSTR} \leq 21\ \mathrm{bar},$

$10\ \mathrm{bar} \leq p_{total}^{PFR}(z) = p_{CO}^{PFR}(z) + p_{H_2}^{PFR}(z) \leq 21\ \mathrm{bar},$

Temperature: $363.15\ \mathrm{K} \leq T_{CSTR} \leq 388.15\ \mathrm{K},$

$363.15\ \mathrm{K} \leq T_{PFR}(z) \leq 388.15\ \mathrm{K},$

Reactor volume: $V_{CSTR} \leq 1\,\mathrm{l}, \varepsilon_{liq}^{CSTR} = 0.3, V_{PFR} = 2.2\,\mathrm{l}, \varepsilon_{liq}^{PFR} = 0.33,$

Controls: $u(t) = \left[T_{PFR}(z), j_{CO}^{PFR}(z), j_{H_2}^{PFR}(z)\right],$

$p = [T_{CSTR}, j_{CO}^{CSTR}, j_{H_2}^{CSTR}, \xi_{rec}^{dec}, \xi_{rec}^{col}].$

A.8 Nomenclature:

Latin symbols

a	parameters	various
c	concentration	mol/ml
d	diameter (of reactor tube)	m, mm
D	dispersion coefficient	m^2/s
$\Delta_R G$	Gibbs energy of reaction	J/mol
Δp	pressure drop	bar/m
ΔS	selectivity difference	-
E_A	activation energy	J/mol
H	Henry coefficient	bar/ml/mol
j	molar flux	mol/min
k, K	chemical reaction coefficient	various
$k_L a$	volumetric mass transfer coefficient	1/s, 1/min
l	length (of reactor tube)	m
M	Molar mass	kg/mol
n	amount of moles	mol
N	number of CSTRs in cascade	-

n/iso	ratio of linear and branched aldehydes	-
p	pressure, optimization parameter vector	bar, -
r	reaction rate	mol $/(g_{cat}min)$
R	universal gas constant	J/mol/K
S	section, selectivity	-
t	time	s
T	temperature	K
u	control vector	-
v	velocity	m/min, m/s
V	volume	m^3
$\dot{V}$	volumetric flow rate	ml/min
w	mass fraction	-
$\hat{x}$	input states of Kriging model	-
X	conversion	-

Greek symbols

ε	hold-up	-
ζ	split factor of distillation column	-
$\hat{\theta}$	fitted Kriging model parameters	-
ν	stoichiometric coefficient	-
φ	differential selectivity	-
ξ	purge factors	-
ρ	mass density	kg/m^3

τ	residence time	-

Abbreviations

AMPL	a mathematical programming language
CO	carbon monoxide
COL	distillation column
CSTR	continuous stirred tank reactor
C10an	n-decane
DEC	decanter
DMF	n-,n-dimethylformamide
DSR	distributed/differential sidestream reactor
EPF	elementary process functions
FPA	flux profile analysis
H_2	hydrogen
HK	heavy key
iC12en	iso-dodecenes
iC13al	2-methyl-dodecanal, iso-aldehydes
IPOPT	interior point optimizer (software name)
KR	Kriging model
LK	light key
nC12an	n-dodecane
nC12en	1-dodecene
nC13al	tridecanal
NLP	nonlinear programming

Pé	Péclet number
PFR	plug flow reactor
Rh	rhodium
SBR	semibatch reactor
STY	space-time yield
TMS	thermomorphic solvent system

Subscripts & Superscripts

α, β	chemical components
$apolar$	stream of apolar solvent
ax	axial
B	bottom
cat	catalyst
col	column
D	distillate
dec	decanter
$distr.$	distributed
eq	equilibrium
f	final
gas	gas
HK	heavy key
in	inlet
$init.$	initial
liq	liquid

LK	light key
max	maximal
min	minimal
out	outlet
P	product
$polar$	stream of polar solvent
R	reactant, reactor
ref	reference value
s	superficial
S	separation
st	storage
t	total
0	initial

Sets

CH	hydrocarbons
GAS	gas components
RCT	reactions
SOL	solvents

References

(1) Behr, A.; Witte, H.; Zagajewski, M. Scale-up durch Miniplant-Technik: Anwendungsbeispiele aus der homogenen Katalyse. *Chemie Ingenieur Technik* 2012, *84*, 694–703.

(2) Behr, A.; Fängewisch, C. Temperature-Dependent Multicomponent Solvent Systems – An Alternative Concept for Recycling Homogeneous Catalysts. *Chem. Eng. Technol.* 2002, *25*, 143.

(3) Haumann, M.; Koch, H.; Hugo, P.; Schomäcker, R. Hydroformylation of 1-dodecene using Rh-TPPTS in a microemulsion. *Applied Catalysis A: General* 2002, *225*, 239–249.

(4) Fang, J.; Jin, H.; Ruddy, T.; Pennybaker, K.; Fahey, D.; Subramaniam, B. Economic and Environmental Impact Analyses of Catalytic Olefin Hydroformylation in CO 2 -Expanded Liquid (CXL) Media. *Ind. Eng. Chem. Res.* 2007, *46*, 8687–8692.

(5) Sharma, A.; Lebigue, C. J.; Deshpande, R. M.; Kelkar, A. A.; Delmas, H. Hydroformylation of 1-Octene Using [Bmim][PF 6]−Decane Biphasic Media and Rhodium Complex Catalyst: Thermodynamic Properties and Kinetic Study. *Ind. Eng. Chem. Res.* 2010, *49*, 10698–10706.

(6) Schäfer, E.; Brunsch, Y.; Sadowski, G.; Behr, A. Hydroformylation of 1-Dodecene in the Thermomorphic Solvent System Dimethylformamide/Decane. Phase Behavior–Reaction Performance–Catalyst Recycling. *Ind. Eng. Chem. Res.* 2012, *51*, 10296–10306.

(7) Kiedorf, G.; Hoang, D. M.; Müller, A.; Jörke, A.; Markert, J.; Arellano-Garcia, H.; Seidel-Morgenstern, A.; Hamel, C. Kinetics of 1-dodecene hydroformylation in a thermomorphic solvent system using a rhodium-biphephos catalyst. *Chemical Engineering Science* 2014, *115*, 31–48.

(8) Hentschel, B.; Kiedorf, G.; Gerlach, M.; Hamel, C.; Seidel-Morgenstern, A.; Freund, H.; Sundmacher, K. Model-Based Identification and Experimental Validation of the Optimal Reaction Route for the Hydroformylation of 1-Dodecene. *Ind. Eng. Chem. Res.* 2015, *54*, 1755–1765.

(9) Hentschel, B.; Peschel, A.; Freund, H.; Sundmacher, K. Simultaneous design of the optimal reaction and process concept for multiphase systems. *Chemical Engineering Science* 2014, *115*, 69–87.

(10) McBride, K.; Kaiser, N. M.; Sundmacher, K. Integrated reaction–extraction process for the hydroformylation of long-chain alkenes with a homogeneous catalyst. *Computers & Chemical Engineering* 2016, DOI: 10.1016/j.compchemeng.2016.11.019.

(11) Dreimann, J.; Lutze, P.; Zagajewski, M.; Behr, A.; Górak, A.; Vorholt, A. J. Highly integrated reactor–separator systems for the recycling of homogeneous catalysts. *Chemical Engineering and Processing: Process Intensification* 2016, *99*, 124–131.

(12) Dreimann, J. M.; Warmeling, H.; Weimann, J. N.; Künnemann, K.; Behr, A.; Vorholt, A. J. Increasing selectivity of the hydroformylation in a miniplant: Catalyst, solvent, and olefin recycle in two loops. *AIChE J.* 2016, *62*, 4377–4383.

(13) Kaiser, N. M.; Flassig, R. J.; Sundmacher, K. Reactor-Network Synthesis via Flux Profile Analysis. *Chemical Engineering Journal* 2017, *submitted*.

(14) Kaiser, N. M.; Flassig, R. J.; Sundmacher, K. Probabilistic reactor design in the framework of elementary process functions. *Computers & Chemical Engineering* 2016, *94*, 45–59.

(15) Freund, H.; Sundmacher, K. Towards a methodology for the systematic analysis and design of efficient chemical processes. *Chemical Engineering and Processing: Process Intensification* 2008, *47*, 2051–2060.

(16) Zagajewski, M.; Dreimann, J.; Behr, A. Verfahrensentwicklung vom Labor zur Miniplant: Hydroformylierung von 1-Dodecen in thermomorphen Lösungsmittelsystemen. *Chemie Ingenieur Technik* 2014, *86*, 449–457.

(17) Coleman, J. W.; Garimella, S. Characterization of two-phase flow patterns in small diameter round and rectangular tubes. *International Journal of Heat and Mass Transfer* 1999, *42*, 2869–2881.

(18) Pedersen, H.; Horvath, C. Axial dispersion in a segmented gas-liquid flow. *Ind. Eng. Chem. Fund.* 1981, *20*, 181–186.

(19) Gruber, R.; Melin, T. Radial mass-transfer enhancement in bubble-train flow. *International Journal of Heat and Mass Transfer* 2003, *46*, 2799–2808.

(20) Zlokarnik, M. *Rührtechnik – Theorie und Praxis*; Springer Verlag: Berlin Heidelberg, 1999.

(21) Yaws, C. *Chemical Properties Handbook: Physical, Thermodynamics, Environmental Transport, Safety & Health Related Properties for Organic & Inorganic Chemical, 1st edition,*; McGraw-Hill Professional, 1998.

Author Information

* Email: Flassig@mpi-magdeburg.mpg.de

NMK and RJF performed simulation and optimizations, MJ performed the experiments, KM supported the overall process modeling and optimization. RJF and KS designed the research project. The manuscript was written through contributions of all authors. All authors have given approval to the final version of the manuscript.

Acknowledgement

This work is part of the Collaborative Research Centre/Transregio 63 “Integrated Chemical Processes in Liquid Multiphase Systems” (Subproject B1) - InPROMPT. Financial support by the Deutsche Forschungsgemeinschaft (DFG, German Research Foundation) is gratefully acknowledged (TRR 63).

TOC graphic: (ca. 4.4cm x 8 cm)